

Accepted for publication in the *Astrophysical Journal*  
07/17/08

## X-ray flares in Orion young stars. II. Flares, magnetospheres, and protoplanetary disks

Konstantin V. Getman<sup>1</sup>, Eric D. Feigelson<sup>1</sup>, Giusi Micela<sup>2</sup>, Moira M. Jardine<sup>3</sup>, Scott G. Gregory<sup>3</sup>, Gordon P. Garmire<sup>1</sup>

gkosta@astro.psu.edu

### ABSTRACT

We study the properties of powerful X-ray flares from 161 pre-main sequence (PMS) stars observed with the Chandra X-ray Observatory in the Orion Nebula region. Relationships between flare properties, protoplanetary disks and accretion are examined in detail to test models of star-disk interactions at the inner edge of the accretion disks. Previous studies had found no differences in flaring between diskfree and accreting systems other than a small overall diminution of X-ray luminosity in accreting systems.

The most important finding is that X-ray coronal extents in fast-rotating diskfree stars can significantly exceed the Keplerian corotation radius, whereas X-ray loop sizes in disky and accreting systems do not exceed the corotation radius. This is consistent with models of star-disk magnetic interaction where the inner disk truncates and confines the PMS stellar magnetosphere.

We also find two differences between flares in accreting and diskfree PMS stars. First, a subclass of super-hot flares with peak plasma temperatures exceeding 100 MK are preferentially present in accreting systems. Second, we tentatively find that accreting stars produce flares with shorter durations. Both results may be consequences of the distortion and destabilization of the stellar magnetosphere by the interacting disk. Finally, we find no evidence that any

---

<sup>1</sup>Department of Astronomy & Astrophysics, 525 Davey Laboratory, Pennsylvania State University, University Park PA 16802

<sup>2</sup>INAF, Osservatorio Astronomico di Palermo G. S. Vaiana, Piazza del Parlamento 1, I-90134 Palermo, Italy

<sup>3</sup>SUPA, School of Physics and Astronomy, North Haugh, St Andrews, Fife, KY16 9SS, Scotland, UK

flare types, even slow-rise flat-top flares are produced in star-disk magnetic loops. All are consistent with enhanced solar long-duration events with both footprints anchored in the stellar surface.

*Subject headings:* open clusters and associations: individual (Orion Nebula Cluster) - planetary systems: protoplanetary disks - stars: flare - stars: magnetic fields - stars: pre-main sequence - X-rays: stars

## 1. INTRODUCTION

A broad consensus has emerged in the past decade concerning the structure and astrophysics of pre-main sequence (PMS) stars. The angular momentum inherited from the collapsing interstellar material is mostly distributed into a rapidly rotating protostar, a Keplerian protoplanetary disk, and frequently the orbital motion of multiple stellar components. The young star interacts with its disk in a complex fashion with accretion and ejection of collimated outflow. It is widely believed that strong magnetic fields generated within the young star mediate this star-disk interaction, truncating the disk and funneling accretion onto limited portions of the stellar surface. These issues are developed in a variety of reviews (e.g., Hartmann 1998; Bouvier et al. 2007; Bouvier & Appenzeller 2007).

It has been difficult, however, to elucidate in detail the nature of the PMS stellar magnetospheres and their role in facilitating star-disk interactions and accretion. Well-developed analytical theory assumes that a dipolar field extends to several stellar radii where the Keplerian orbits and stellar fields are in co-rotation, interacts with the disk magnetic field, and guides both accretion onto the surface and into a high-velocity collimated outflow (e.g., Shu et al. 1994; Lovelace et al. 1995). However, considerable evidence has emerged that the magnetic fields on the surfaces of PMS stars are concentrated in complex multipolar active regions similar to those on the Sun, rather than a simple dipolar. This emerges from photometric, Doppler imaging, circular polarization and spectroscopy of Zeeman-sensitive lines from PMS photospheres (e.g., Daou et al. 2006; Yang et al. 2007; Johns-Krull 2007; Donati et al. 2007). Recently, theoretical efforts have begun to calculate the resulting complex PMS magnetosphere and accretion process (Jardine et al. 2006; Gregory et al. 2006a; Long et al. 2007).

X-ray studies are a potentially useful tool for investigating these issues. It has long been known that late-type stars exhibit their highest levels of X-ray emission, arising mostly from violent magnetic reconnection events, during their PMS phase (e.g., reviews by Feigelson & Montmerle 1999; Feigelson et al. 2007). Recent X-ray surveys of nearby PMS stellar populations give

detailed insights into PMS magnetic flaring; these include the Chandra Orion Ultradeep Project (COUP, Getman et al. 2005a) and the XMM/Newton Extended Survey of Taurus (XEST, Güdel et al. 2007). Both astrophysical study of the properties of individual flares, and statistical study of many flares, from the COUP and XEST observations reveal that most events are similar to solar magnetic flaring but with X-ray luminosities enhanced  $10^3 - 10^5$  fold in intensity (e.g. Favata et al. 2005; Wolk et al. 2005; Flaccomio et al. 2005; Stassun et al. 2006; Maggio et al. 2007; Caramazza et al. 2007; Arzner et al. 2007; Stelzer et al. 2007; Franciosini et al. 2007).

The decay of PMS X-ray flares on timescales of  $10^3 - 10^5$  s have proved particularly amenable to astrophysical modeling. One favored model, developed by Reale et al. (1997) and extensively applied to solar and stellar X-ray flares, considers the X-rays produced by thermal plasma at  $T \sim 10^7$  K confined in a cylindrical loop cooling by radiation and conduction but subject to possible reheating by later magnetic reconnection events. Using such models, inferences can be made concerning magnetic fields responsible for the flare, including loop length and magnetic field strength. For the most powerful PMS flares, inferred loop lengths reach  $4 - 20 R_*$ , comparable to the expected inner edges of protoplanetary disks (Favata et al. 2005)<sup>1</sup>. Thus, X-ray flaring potentially probes the region of star-disk interaction. Links are also emerging between other features of PMS X-ray emission, such as the statistical suppression of flares in accreting systems and the rotational modulation of X-rays, and models of multipolar PMS magnetospheres (Gregory et al. 2006b, 2007).

The present study extends the analysis of powerful flares from the COUP made by Favata et al. (2005). They modeled 32 flares using a traditional technique of time-resolved spectroscopy. In Getman et al. (2008, Paper I) and Getman et al. (2006), we introduce a more sensitive data analysis method based on adaptively smoothed median energies which permits modeling of 216 COUP flares. This is a sufficiently large sample that permits new investigation of possible links between flaring, PMS magnetospheres and protoplanetary disks. Here, we present observational evidence that X-ray emitting coronal structures are in fact truncated by inner disks around the Keplerian corotation radius, just as predicted by PMS theoretical models outlined above. We also report a variety of other results, both positive and negative, linking magnetic flare properties to the presence or absence of disks.

The paper is organized as follows. Preliminary work and recovery of some established results are given in §2. The main results of our study appear in the following three sections: the absence of strong links between some flare properties and disks (§3); clear evidence that

---

<sup>1</sup>Recall, however, that the vast majority of weaker PMS flares arise in magnetic loops no larger than the star (e.g. Imanishi et al. 2003; Wolk et al. 2005; Franciosini et al. 2007).

PMS magnetospheres do not extend beyond disk inner edges (§4); and possible relations between super-hot flares, accretion and non-dipolar magnetic fields (§5 and 6). Discussion follows in section §7. Readers are encouraged to consult Paper I for details on the selection, modeling, and properties of the 216 COUP flares discussed here.

## 2. PRELIMINARY CONSIDERATIONS

### 2.1. Disk and accretion indicators

We follow a well-established path in defining the presence of disks and accretion in PMS stars. The  $K_s$ -[3.6]-[4.5] color-color diagram on Figure 1 shows 98 sources with available IR photometry (both  $\Delta(H - K_s)$  and [3.6] – [4.5]; see Table 4 of Paper I). This diagram is known to provide good discrimination between Class I (protostellar), Class II (classical T Tauri) and Class III (weak-lined T Tauri) systems (e.g. Hartmann et al. 2005). The reddening vector of  $A_V \sim 30$  mag for a diskfree Vega-like spectrum assuming the reddening law of Mathis (1990) demarcates the locus of Class III objects to the left from the Class II and Class I systems to the right. All COUP 98 objects, except for three with their color [3.6] – [4.5] > 0.5, have their inferred X-ray column densities  $\log N_H < 22.3 \text{ cm}^{-2}$  (Table 4 of Paper I). For normal interstellar gas-to-dust ratios, this corresponds to a visual absorption of < 10 – 12 mag (Vuong et al. 2003) and thus to the limiting color of [3.6] – [4.5] < 0.2 for Class III objects. Several stars to the left of the reddening vector and with [3.6] – [4.5] color in excess of 0.2 may be systems with either higher photometric errors and/or special reddening conditions in their individual star-disk systems. Nevertheless, the rough mid-infrared (MIR) color criterion of [3.6] – [4.5] = 0.2 effectively discriminates between Class III and Class II systems, and we use this as our main MIR disk indicator. A few COUP sources with  $K_s - [3.6] \sim 2$  may be Class I or transitional Class I/II systems. One of them, COUP #570, is classified as 0/Ib protostellar candidate in Prisinzano et al. (2007).

$\Delta(H - K_s)$  near-infrared (NIR) excess is an indicator of a heated inner dusty circumstellar disk. It is measured from the reddening vector on  $J - H$  versus  $H - K_s$  diagram of COUP sources (e.g. Figure 5a in Favata et al. 2005) adopting photospheric colors associated with PMS stars at age 1 Myr using the models of Siess et al. (2000), and considering a reddening vector applied to 0.1  $M_\odot$  stars. Only four sources in our sample have masses  $M < 0.2 M_\odot$ , but 40 have  $0.2 < M < 0.4 M_\odot$ . In order to allow better discrimination of inner disks, we can relax the criterion  $\Delta(H - K_s) = 0$  mag to the value in the range of (–1, –0.06) mag corresponding to reddening vectors at the mass range of 0.2 – 0.4  $M_\odot$ .

Using this NIR color excess measure, we find that a criterion of  $\Delta(H - K_s) = -0.06$  mag

is a good discriminator between diskfree and disk stars established with the MIR color criterion of  $[3.6] - [4.5] = 0.2$ ; 95% of sources classified as Class III using this MIR color criterion are also Class III using our NIR color criterion (Figure 1). About 17 stars are classified as Class II systems using MIR colors but Class III using NIR colors; these systems likely have evolved disks with inner holes.

Discrimination between accreting and non-accreting objects employs the equivalent width of the IR 8542 Å Ca II line,  $EW(\text{Ca II})$ , measured from low-resolution spectroscopy by Hillenbrand (1997). In Figure 2, we adopt the classification criterion used by Flaccomio et al. (2003): stars with the line in emission with  $EW(\text{Ca II}) < -1$  Å are accretors while stars with the line in absorption and equivalent width of  $EW(\text{Ca II}) > 1$  Å are considered to be non-accretors. Stars with intermediate values  $-1 < EW(\text{Ca II}) < 1$  Å have an indeterminate classification. Figure 2 shows that this  $EW(\text{Ca II})$  accretion indicator agrees in most cases with the  $\Delta(H - K_s)$  NIR inner disk indicator: inner disk photometric excess is seen in 15 of the 19 accretors and no photometric excess is seen in 32 of the 41 non-accretors. COUP flaring sources with their conservatively chosen  $EW(\text{Ca II}) < -2$  Å will be further classified in the text as high-accretors<sup>2</sup>.

Recall that photometric and inferred properties (such as age, mass and rotation) for these COUP stars are tabulated by Getman et al. (2005a), and tables in Paper I present various observed and inferred stellar and flare quantities. Tables 1 and 2 of the current paper give general statistical properties of those quantities. They also provide probabilities  $P_{KS}$  from two-sample univariate Kolmogorov-Smirnov tests comparing the distributions of various quantities in diskfree and disk stars. Significant disk effects may be present when  $P_{KS} \lesssim 0.05$ . This is relevant for such quantities as rotational period, Keplerian corotation radius, peak flare plasma temperature, coronal loop size relative to stellar radius, and X-ray coronal extent relative to corotation radius.

## 2.2. Disks and stellar rotation

Using our sample of X-ray bright COUP stars, we confirm the well-established result that Orion Nebula Cluster PMS stars with disks rotate slower than those without disks (e.g.,

---

<sup>2</sup>The association between accreting stars and MIR-excess stars in our sample is not perfect. Four high accretors located at the outskirts of the *Chandra* field are not part of the MIR disk sample because they lie outside the *Spitzer* IRAC fields from which we obtained MIR photometry. An additional high accretor lies projected against the infrared-bright BN/KL region which is classified as a diskfree star based on its (possibly erroneous) MIR photometry. See also §2.3 and Figure 4.

Herbst et al. 2002; Rebull et al. 2006). Our rotational periods are obtained from published sources but our MIR photometry was derived independently from *Spitzer Space Telescope* data as described in Paper I and our classification of disk versus diskfree stars was determined as described above.

This expected result is shown in Figure 3 where stars with MIR disks (blue circles) and accretion (green boxes) systematically have longer periods and larger corotation radii<sup>3</sup> than diskfree stars (red circles). This supports the explanation that slow PMS rotation is due to the loss of a stellar angular momentum through a magnetic star-disk interaction (see review by Bouvier et al. 2007). Table 1 shows that the rotational periods of our bright X-ray flaring stars are well-separated with a median of 9.0 days for those with MIR disks compared to 3.5 days for those without MIR disks. Rotation of our accreting systems are not distinguishable from other stars with MIR disk. It is useful to note that the range of COUP rotational periods of  $[1 - 10]$  days translates into the range of corotation radii of  $[2 - 10]$   $R_\star$  with the majority of COUP stellar radii in  $[1.4 - 3]$   $R_\odot$  range (Figure 3).

### 2.3. Disks and location in the cloud

Figure 4 shows the spatial distribution of our stars with and without MIR disks in the Orion Nebula region. The region is complicated: the rich, optically bright Orion Nebula Cluster has low absorption and lies in front of the two OMC 1 molecular cloud cores, as well as widely distributed molecular cloud material, where PMS stars are highly absorbed. In the figure, the stars are coded both by their disk properties and by their absorption measured from the soft X-ray absorption in their COUP spectra (Getman et al. 2005a). The spatial distribution of the COUP stars is further discussed by Feigelson et al. (2005) and Prisinzano et al. (2007).

Bright flaring COUP stars with MIR disks and the highest absorption (blue circles in panel *a*) are largely concentrated around OMC 1 molecular filament to the north of the Becklin-Neugebauer star forming region. Those with intermediate absorption have a somewhat broader distribution centered north-east of the OMC cloud cores. The diskfree stars in our sample are generally less absorbed than those with MIR disks with a dispersed spatial distribution similar to the diskless stars with intermediate absorption (Figure 4*b*). For both samples, stars harboring super-hot ( $T_{obs,pk} > 100$  MK, see § 5) flares are localized within the north-eastern part of the cloud. The high accretors appear widely dispersed (Figure 4*c*),

---

<sup>3</sup>Recall that Keplerian corotation radii for stars with known rotational periods  $P$  and masses  $M$  are calculated in Paper I as  $R_{cor} = (GMP^2/4\pi^2)^{1/3}$ .

but this is a selection effect - only 12 high accretors have their observed X-ray net counts above the count threshold of our flare analysis ( $NC = 4000$  counts, see Paper I and footnote 2). The total known population of COUP high accretors have spatial distribution similar to that of the bright flaring COUP MIR disk stars with intermediate absorption (Figure 4d).

### 3. FLARE PROPERTIES AND PROTOPLANETARY DISKS

Paper I presents in detail our analysis of the selected COUP flares and the derivation of flare properties used in the analysis here: rise and decay timescales, “characteristic” pre-flare and peak flare X-ray luminosities, peak flare plasma temperature and emission measure, flare morphology, and magnetic loop length responsible for the flare. These quantities are derived using the astrophysical model of flare decays developed by Reale et al. (1997). This is a single loop model and is simplistic in a number of ways (see its limitations in sections 2.2 and 2.5 of Paper I). However, even in the case of complex flares, it is appropriate to apply the model to a lightcurve segment if there is an indication for the presence of a single “dominant” flaring structure (see sections 2.5 and 2.6 of Paper I).

Adopting the model of Reale et al., Favata et al. (2005) have analysed the strongest 32 COUP flares using the long-standing flare analysis method of time-resolved spectroscopy (TRS). To extend the flare sample of Favata et al. (2005), Paper I utilizes a more sensitive technique of flare analysis, the “method of adaptively smoothed median energy” (MASME), introduced by Getman et al. (2006). Instead of performing classical TRS with XSPEC over only a few characteristic flare intervals, we employ an adaptively smoothed estimator of the median energy of flare counts and count rate to infer the evolution of plasma temperature and emission measure at dozens of time points along the decay phase of a flare. This is achieved by calibrating median energies and count rate to temperatures and emission measures through simulations of high signal-to-noise spectra at fixed source’s column density. The method permits modeling of flare spectra on more rapid timescales and with weaker signals than was possible using traditional spectral fitting. Readers are encouraged to consult section 2.2 and Appendices A and B of Paper I on details of the method. The result is that Paper I characterizes 216 COUP flares for analysis here, in contrast to 32 flares analyzed by Favata et al. (2005).

### 3.1. Disks have no effect on flare morphology

Paper I describes our qualitative classification of X-ray flares by their lightcurves during the flare. The four classes are: ‘typical’ flares with fast rises and slower decays characteristic of most solar flares; ‘step’ flares with extra emission during the decay attributable to a reheating or a secondary reconnection event; ‘double’ flares with two peaks suggestive of two nearly simultaneous reconnection events; and ‘slow rise, top flat’ (SRTF) flares. The first three classes are commonly seen in solar flares. For example, Figure 11 of Paper I shows solar flares with secondary events during the decay of powerful long-duration events. Such events, scaled up several orders of magnitude, could be classified as step or double flares in COUP lightcurves.

The SRTF flares are more unusual, and one may speculate that they may be selectively formed in certain PMS stars. For example, they might be reconnection events associated with sheared star-disk magnetic fields (Montmerle et al. 2000; Isobe et al. 2003) rather than events associated with field lines attached to the star. Flare morphology is coded by different symbols in Figures 2, 6, 7 and 8. We examine here the distribution of flare types along the abscissa measuring the strength of accretion, NIR inner disk, and MIR disk indicators. No pattern between flare morphology and disk indicators is seen. In particular, SRTF flares are seen in systems with and without MIR and NIR disks. However, SRTF flares are not seen in high-accretion systems; this can be an indication of a real physical effect (§3.2) or simply attributed to the very limited statistics of both accreting and SRTF flare samples.

### 3.2. Disks are unrelated to flare energetics

We examine here whether any relationships are present between disks and quantities associated with the strength of the X-ray flares: rise and decay timescales, peak luminosities, and total energies in the X-ray bands.

Figure 5 *a-b* show the distributions of flare rise and decay times stratified by disk and accretion properties. There is a hint that high-accretors have systematically shorter flare timescales compared to the rest of the bright COUP flare sample. The evidence is only suggestive because our sample of high-accretors is small (17 flares from 12 sources) and it is only marginally significant when measured by a KS test ( $P = 0.06$  when rise times for high-accretors are compared to diskfree systems). Figure 5 *c* shows that the distribution of flare peak luminosities are indistinguishable for diskfree, MIR disk, and accretion disk systems.

We evaluate the total energies of each of the 216 flares as the difference between the



time-integrated flare energy  $E_{flare}$  and the energy from the non-flare “characteristic” state  $E_{char}$  within the duration of the flare,  $t_{flare2} - t_{flare1}$ . We estimate  $E_{flare} \approx L_{X,pk} \times \tau_{decay2}$  and  $E_{char} = L_{X,char} \times (t_{flare2} - t_{flare1})$ , where X-ray luminosity from the “characteristic” state,  $L_{X,char}$ , was taken from our TRS analysis (Paper I).  $E_{char}$  is systematically lower in flares from high-accretors (panel *d*); this is due to the shorter flare durations (above) and lower  $L_{X,char}$  in accreting systems<sup>4</sup>. The latter effect is the well-established suppression of time-integrated X-ray emission in accreting vs. non-accreting PMS systems (Gregory et al. 2007, and references therein). Due to shorter flare timescales,  $E_{flare}$  in high-accretors shows a somewhat narrower distribution than that of other stars but the difference is not statistically significant (panel *e*).

A more interesting effect is seen in the ratio  $E_{flare}/E_{char}$  which is systematically larger in high-accretors than other stars. The median value  $E_{flare}/E_{char} \simeq 10$  compared to 5 in diskfree stars ( $P_{KS} = 0.008$ , Figure 5*f*). In the 840 ks of the COUP observation, a typical single bright flare with a duration of 90 ks (median of  $t_{flare2} - t_{flare1}$  for all 216 flares) may increase the time-integrated source X-ray luminosity 1.5 – 2 times if  $E_{flare}/E_{char} = 5 - 10$ . For a shorter more typical *Chandra* exposure, a 50 ks bright flare ( $< 22\%$  of flares analyzed here have durations  $< 50$  ks) will change the time-integrated source X-ray luminosity 3 – 5.5 times if  $E_{flare}/E_{char} = 5 - 10$ .

The major result of the section is that no difference is found in flare duration, peak luminosity and total energy between flares occurring in disk and diskfree systems. However, as a tentative finding flares from high-accreting disk stars seem to be somewhat shorter and thus have weaker total X-ray energies than the rest of the analyzed flares. This tentative finding is supported by two statistically significant findings: 1. super-hot COUP flares are found to be shorter than cooler COUP flares (Paper I) and 2. super-hot flares preferentially present in accreting systems (§5).

#### 4. DISKS MAY TRUNCATE PRE-MAIN SEQUENCE MAGNETOSPHERES

Figures 6, 7 and 8 compare the flare loop lengths inferred from analysis of the X-ray spectral evolution of the decay phases (Paper I) with our disk and accretion indicators. After

---

<sup>4</sup>In our flare sample the effect of lower  $L_{X,char}$  in accreting systems is not strong. A KS test gives only marginally significant difference ( $P_{KS} = 0.1$ ) in  $L_{X,char}$  between high-accretors and diskfree stars. Median values of  $\log(L_{X,char})$  are 30.16 erg s<sup>−1</sup> for diskfree stars, 30.10 erg s<sup>−1</sup> for MIR disk stars, and 30.10 erg s<sup>−1</sup> for high-accretors.

careful investigation of various measures of magnetospheric size, we choose to examine the ratio of the coronal extent of the loop as measured from the star center,  $L + R_\star$ , to the Keplerian corotation radius  $R_{cor}$  determined by the stellar rotation rate. We are thus less interested in the loop size measured in meters than the relative sizes of the loop to the likely location of the inner edge of the disk. This measure reduces variations associated with star mass, age and rotation and focuses on the question of the relationship between PMS disks and magnetospheres.

Figure 6 plots  $(L + R_\star)/R_{cor}$  against the NIR  $\Delta(H - K_s)$  disk indicator. The vertical lines for each flare do not represent error bars, but are the low and upper boundary of the inferred loop size ranges (Paper I) with symbols positioned at the mean of those ranges. We find that, except for COUP # 1608<sup>5</sup>, coronal structures responsible for flares detected from a dozen sources with NIR inner disks do not exceed  $R_{cor}$ , while coronal structures responsible for  $\sim 40\%$  of flares from 43 sources without NIR inner disks exceed  $R_{cor}$ . Some of these flares in diskfree systems arise from loops reaching  $\gtrsim 2 \times R_{cor}$ . This pattern is present in each morphological flare type (typical, step, double, slow rise/flat top) as indicated by different symbols.

The same pattern is seen when  $(L + R_\star)/R_{cor}$  is plotted against the MIR disk indicator  $[3.6] - [4.5]$  (Figure 7) and the accretion indicator EW(Ca II) (Figure 8). Virtually all of the flares whose inferred sizes exceed the host star’s corotation radius are diskfree and non-accreting systems, while diskgy and accreting flare loops all lie within the corotation radius. The MIR plot adds nine flares from five sources which were not available in the NIR plot; all of these follow the NIR trend. Two outliers, COUP #205 and 485, are those for which inner part of the disk is likely cleared of circumstellar material (judging from their NIR colors). Again, the trend is strong and applicable to each morphological type of flares. The sample of stars with strong EW(Ca II) emission indicating active accretion is smaller than those with infrared photometric excesses, but the trend of smaller loop sizes in accreting systems is still clearly seen.

These three figures provide strong and consistent support for a model where protoplanetary disks truncate PMS magnetospheres. We do not know of any selection effect that would have produced this pattern in a spurious fashion. The plots in Figure 9 help elucidate this trend. Here the symbol colors represent the classification of diskgy (blue) and diskfree (red) stars based on MIR colors, and only the mean value of inferred flare loop size is shown. Recall from Figure 3 that, due to the well-established connection between disks and rota-

---

<sup>5</sup>This outlier is a visual double unresolved by 2MASS, and we suspect the NIR photometry is unreliable. It lies outside the field of the *Spitzer* IRAC images, so its MIR properties are unavailable.

tion, corotation radii scaled to stellar radii are systematically larger for diskfree compared to diskfree stars (the difference is roughly a factor of two). This difference in  $R_{cor}/R_*$  is the major contributor to the difference in  $(L + R_*)/R_{cor}$  between the diskfree and diskfree stars seen in Figures 6-8. If the loop sizes  $L/R_*$  were to be considered without normalization to the corotation radii, the difference between the two classes becomes marginal<sup>6</sup>.

We thus find that X-ray coronal extents are somewhat similar in diskfree and diskfree systems but, due to the well-established fact that diskfree stars are faster rotators, the X-ray flares often exceed the corotation radius in these systems. In contrast, X-ray flare loops on diskfree stars never exceed the corotation radius, although in some cases they reach the corotation radius which is also the likely truncation radius for the circumstellar disk. The fact that X-ray loops of diskfree stars are close to but never exceed **the one corotation radius** supports long-standing models of star-disk magnetic interaction at this inner edge involving accretion, outflow ejection, and regulation of the stellar angular momentum. The very large loop sizes seen in all types of PMS stars point to confinement by strong magnetic fields of T-Tauri stars which, particularly in rapidly rotating diskfree systems, are capable of withstanding the effects of centrifugal forces (Jardine & Unruh 1999).

## 5. Super-hot flares and disks

Paper I describes the selection of 73 of the 216 COUP flares as ‘super-hot’ with peak plasma temperatures  $T_{pk} \gtrsim 100$  MK. Similar flares have been occasionally reported in other PMS systems such as the diskfree binary PMS star system V773 Tau observed with ASCA (Tsuboi et al. 1998), two embedded young systems in the NGC 2264 star forming region (Simon & Dahm 2005), and about half of the COUP flares studied by Favata et al. (2005). However, here we have a sufficiently rich sample to study super-hot PMS flares as a class. This is made possible by the large Orion population, the unusually long COUP exposure, and our new highly-sensitive flare analysis techniques.

There is some concern that the *Chandra* telescope cannot discern differences in plasma temperatures above  $\sim 100$  MK due to the rapid decline in mirror reflectivity above  $\sim 8$  keV. However, we explain in detail in Appendix B of Paper I and the Appendix below that, when high-signal flares are considered, that discriminations between 100 MK and  $\gtrsim 200$  MK

---

<sup>6</sup>To avoid observational bias of Class III stars towards higher  $R_{star}$  and thus restricting the flare sample to stars with stellar radius in the range of  $R_* = [1 - 3] R_\odot$  gives the following results: KS test shows no statistical difference ( $P_{KS} = 0.2$ ) in  $L/R_*$  between Class II and Class III; median values of  $L/R_* = 3.2(2.4)$  for Class II(III) suggest that  $L/R_*$  in Class II stars is 1.3 times larger than that of Class III.

peak temperatures as well as between  $\lesssim 100$  MK and  $\gtrsim 100$  MK are possible using the median energy as a temperature indicator (our MASME technique described in Paper I). We argue that  $\gtrsim 200$  MK super-hot peak temperatures were missed by the more traditional time-resolved spectroscopy techniques.

To check on the applicability of the Reale model to unusually large and hot loops the detailed time-dependent hydrodynamic simulation was applied to a typical super-hot flare of the COUP source #1343 with observed peak flare temperature of a few-to-several hundred MK and derived sizes of associated coronal flaring structures of  $\sim 10^{12}$  cm (section 4.1 in Favata et al. 2005). The model achieved peak temperature of  $\sim 200$  MK and matched both, the observed flare spectrum and lightcurve. The loop plasma was heated rapidly to  $\sim 200$  MK on time-scale of 1 hour following by explosive chromospheric evaporation with chromospheric plasma reaching the loop apex on similar time-scale of 1 hour. This was followed by the decay phase from the nearly equilibrium state governed by conduction and radiation cooling processes on a time-scale of a few to several hours.

Table 2 shows that the flare peak temperatures of stars with MIR disks are systematically higher than peak temperatures for stars without MIR disks at high statistical significance ( $P_{KS} = 0.9\%$ ). It is not clear why the effect is not seen in  $K$ -band excess systems. Figure 10a shows that this effect is even more prominent when disk-free stars are compared to high accreting stars based on the Ca II emission line indicator for accretion. Flares from MIR-excess disk stars (solid black distribution) are on average hotter than those from non-disk stars (dotted) and, among flares from disk stars, those from high-accretors (dashed) are the hottest. As a consequence, high-accretors have the largest fraction of super-hot ( $T_{obs,pk} > 100$  MK) flares (53%) compared to that of stars with MIR disks (40%) and diskfree stars (27%). The effect of systematically hotter flares in disk and highly accreting stars becomes even more prominent (at a significance level of  $P_{KS} = 0.02\%$ ) when only flares from  $M < 2 M_{\odot}$  stars are considered (Figure 10b). Even when uncertainties on individual values of  $T_{obs,pk}$  (which can be large for very high temperatures; Appendix B in Paper I) are taken into account through Monte-Carlo simulations, this significance level does not exceed  $P_{KS} = 1.5\%^7$ . We thus find strong evidence that super-hot flares are preferentially associated with PMS stars undergoing substantial accretion.

Disk stars which possess super-hot flares, including accretors, tend to have spectral

---

<sup>7</sup> We simulated and compared 10000 temperature distributions for each of the sample (diskless, disk and high-accretors), with individual temperature values randomly drawn from Gaussian distributions with mean equal to the measured  $T_{obs,pk}$  and variance as an average error reported in Appendix B of Paper I. We find that (50%, 68%, 90%) of 10000 resulting significance levels from both, the K-S tests between diskless vs. disk and diskless vs. high-accretors comparisons, do not exceed values of  $P_{KS} = (0.3\%, 0.5\%, 1.5\%)$ , respectively.

types late-K and M corresponding to masses  $M \lesssim 1 - 2 M_{\odot}$ , while the majority of diskfree stars with super-hot flares are more massive with spectral types early-K through F (thin dashed line in Figure 10b). This latter group is not large: for sources with known masses, 66% of the super-hot flares are produced by stars with  $M < 1 M_{\odot}$  while only 15% are produced by stars with  $M > 2 M_{\odot}$ . This can be attributed to the rarity of intermediate-mass stars compared to lower mass stars in the Initial Mass Function<sup>8</sup>. The bottom line seems to be that in low-mass stars ( $M < 1 M_{\odot}$ ) the appearance of super-hot flares is connected to the presence of active (accreting) disks, however super-hot flares may also arise in massive ( $M > 2 M_{\odot}$ ) diskfree stars.

## 6. Magnetic fields geometries

Our analysis can provide indirect access to the geometry and strength of the large-scale magnetic fields responsible for confining the X-ray emitting plasma during the bright PMS flares studied here. As described in Paper I, the flare decay model gives estimates of the flare plasma peak emission measure ( $EM_{pk}$ ), coronal loop size (we use here the mean value of the size range,  $L$ ), and plasma temperature ( $T_{obs,pk}$ ). If we add an assumption concerning the ratio of the cylindrical loop cross-sectional radius to the loop length  $\beta$ , we can derive the plasma electron density  $n_e$  from the emission measure and loop length. The magnetic field confining the plasma can then be estimated assuming pressure equilibrium,

$$B_{eq} \simeq (8\pi \times 2n_e k T'_{pk})^{1/2} \text{ where } n_e \simeq (EM_{pk} / (2\pi\beta^2 L^3))^{1/2}. \quad (1)$$

Following past flare models, we adopt a 10:1 cylindrical geometry,  $\beta = 0.1$ .  $T'_{pk}$  used here is the plasma temperature at the loop apex, which is hotter than the observed X-ray temperature integrated over the entire loop according to  $T'_{pk} = 0.068 \times T_{obs,pk}^{1.2}$  where both temperatures are in units of K (Reale 2002; Favata et al. 2005).

Figure 11 shows the resulting inferred plasma densities (panel *a*) and magnetic field strengths (panel *b*) for all (147 of the 162) flares with known loop sizes and stellar radii of their host stars. Plasma density  $n_e$  is anticorrelated with the loop size  $L$  as expected from equation (1); the grey line shows the relation  $n_e \propto L^{-3/2}$  expected for constant emission

---

<sup>8</sup>Out of 161 COUP stars analyzed here 83 have known masses of  $M < 1 M_{\odot}$  and 23 have masses of  $M > 2 M_{\odot}$ . Out of 57 stars producing super-hot flares 27 have known masses of  $M < 1 M_{\odot}$  and 7 have masses of  $M > 2 M_{\odot}$ . The fraction of low-mass super-hot stars (27/83) is comparable to that of higher-mass stars (7/23).

measure and stellar radius. Estimated plasma densities<sup>9</sup> range from  $4 \times 10^9 \text{ cm}^{-3}$  for very large loop sizes ( $L \sim 10 R_\star$ ) to  $1 \times 10^{12} \text{ cm}^{-3}$  for small loop sizes of  $L \lesssim 0.2 R_\star$ .

Figure 11*b* plots the equilibrium magnetic field strengths obtained from equation (1) of individual COUP flares against the inferred flare loop lengths. But the relationship between magnetic field strength and loop length is also a function of field geometry. The simplest geometry often assumed for PMS stars is a dipole,

$$B = \frac{B_{ph}}{(L/R_\star + 1)^3} \quad (2)$$

where  $B_{ph}$  is the photospheric magnetic field which can be directly measured. Figure 11*b* shows these relations for several photospheric field strengths in the range 1 – 6 kG consistent with measurements of Zeeman broadening and circular polarization of PMS photospheric lines (Johns-Krull et al. 1999; Symington et al. 2005; Johns-Krull 2007; Donati et al. 2007).

Figure 11*b* shows that for most of the flares the magnetic fields estimated assuming pressure equilibrium are consistent with the assumption of dipole geometry with photospheric magnetic strengths comparable to the observed values of 1 – 6 kG. These include all types of systems: diskfree stars (red circles), MIR disk stars (blue circles), active accretors (green boxes), and higher mass stars (black triangles). Thus the majority of the flares from our flare sample are associated with the extended, dipole-like loops, and as already discussed in Paper I are different from the previously reported smaller stellar flares which take place in the complex surface field regions likely making up the “characteristic” level of X-ray emission.

However about 40 flares have inferred field strengths too strong for their inferred loop lengths and/or have loop lengths too long for any realistic dipole model. Nearly all of these discrepant flares have super-hot peak temperatures (magenta circles in Figure 11(b)). If a dipolar topology and pressure equilibrium holds, the implied surface magnetic field is tens of kilogauss, far above reasonable values.

This discrepancy can not be fully explained by uncertainties in inferred peak flare temperatures. Both Appendix B of Paper I and the Appendix below provide detailed evidence that the existence of super-hot peak temperatures with  $T_{obs.pk} > 100 \text{ MK}$ , and often  $> 200 \text{ MK}$ , is reliable. The uncertainties of these super-hot temperatures shown in Figure 15 of Paper I propagate into loop size uncertainties of 40% and magnetic strength uncertainties

---

<sup>9</sup> We note that the highest loop plasma densities derived here from modeling flare events are comparable to the high densities inferred from high-resolution X-ray spectra which are usually attributed to shocks at the base of accretion streams (e.g., Kastner et al. 2002; Schmitt et al. 2005; Drake et al. 2005; Argiroffi et al. 2007; Güdel & Telleschi 2007; Huenemoerder et al. 2007). This indicates that plasma density alone may not be a reliable discriminant between flare and accretional X-rays.

of 10%. The confidence regions of most super-hot flares in Figure 11b thus lie above the locus of dipolar fields with photospheric strength of  $B_{ph} \sim 10$  kG.

As discussed in §5, super-hot flares appear to be associated with the presence of a disk and high accretion. We thus emerge with evidence for anomalous magnetic fields associated with accreting PMS stars. Super-hot flares typically arise in large coronal loops  $L/R_\star \gtrsim 2$  but still inside the corotation radius. In §7.1, we speculate that such anomalous fields may result from the distortion of magnetic topologies or the thickening of magnetic loops by the process of accretion.

## 7. Discussion

### 7.1. Does flaring occur in star-disk magnetic fields?

The first result we encounter in this study is negative: disks appear to have no effects on flare morphology, timescales, or energetics (§3.1-3.2). This is not a trivial finding; there is no reason to believe that flares arising in field lines attached to the inner rim of the circumstellar disk would have the same power, plasma properties and temporal evolution as flares from magnetic loops anchored in the stellar surface. Reconnection in star-disk loops can occur in several ways: by magnetic interactions between star and disk fields near the corotation radius (Hayashi et al. 1996), by stochastic fluctuations in the accretion rate near the corotation radius (Shu et al. 1997), or by twisting of star-disk loops from stars slightly out of corotation with their disks (Birk et al. 2000; Montmerle et al. 2000). Isobe et al. (2003) calculated the hydrodynamical response of cool plasma to a sudden reconnection event in the middle of  $1 \times 10^{12}$  cm star-disk loop. They find that the shock reaches both the stellar and disk surfaces in 1 – 2 hours with bulk plasma motions sometimes exceeding 1000 km s<sup>-1</sup>. Temperatures quickly reach 50 – 100 MK but the rise in emission measure sometimes appears slower and less regular than in typical solar-type flares. These might be classified as slow-rise-flat-top or double flares. Remarkably, Isobe et al. find that the entire inner disk gas can be vaporized by powerful reconnection events.

Thus, although SRTF and double flares conceivably could arise exclusively in star-disk loops, our results indicate this is not the case. Instead, we find that all flare morphological types occur equally in both diskfree and disk systems with similar luminosity and duration distributions. We therefore conclude that all flare types likely arise in traditional solar-type magnetic loops where both footprints are rooted in the stellar surface. This idea is supported by the similarity of COUP flaring statistics and plasma elemental abundance anomalies to those seen in older magnetically active stars (Wolk et al. 2005; Maggio et al.

2007; Stelzer et al. 2007). Figure 11 in Paper I shows that step and double flares are commonly seen in the contemporary Sun, often because of a triggered reconnection or a reheating event. Slow-rise-flat-top flares may be similar to other flares with reconnection sequentially progressing along multiple magnetic arcades. Thus, all types of COUP flares may arise from solar-type magnetic morphologies.

However, the solar-type flare analogy to powerful, long-lasting COUP flares faces a challenge. Jardine & Unruh (1999) has raised the issue that very large magnetic loops anchored to rapidly rotating stars may be destroyed when the centrifugal force of their confined plasma exceeds the weakening magnetic tension in the outer part of the loop. Favata et al. (2005) considered this instability to be a strong argument in favor of attaching long loops to the circumstellar disks. We tentatively conclude from our findings that, while this centrifugal force might break some magnetic loops, others survive to produce the observed powerful flares in diskfree high rotating COUP stars.

There is one flare parameter which is linked to the presence of a disk: flares on Class II and high-accretion stars have systematically hotter peak flare temperatures (§5 and Table 2). This may point to star-disk reconnection as modeled by Isobe et al. (2003) where temperatures of 100 MK are easily achieved. Additional calculations should be made to establish the conditions where peak temperatures of 200 MK or more occur. However, it is also possible that these higher temperatures are a byproduct of systematically higher surface magnetic fields in Class II systems which would be capable of confining hotter plasmas. Younger systems might have stronger fields due to vigorous dynamo precesses (Browning 2007), a primordial field component (Johns-Krull 2007), and/or accretional processes (Bessolaz et al. 2008). Hotter peak temperatures could be a byproduct of the magnetosphere compression by disks discussed in §7.2, or atypical coronal loop geometries with larger aspect ratios than typical of solar coronal loops,  $\beta \gg 0.1$ . Rare examples of such “thick” stellar coronal loops are reported in the literature; for example, the AB Dor 29 Nov 1997 flare has estimated  $\beta \sim 1$  (Maggio et al. 2000; Reale 2007). We conclude that the correlation between peak flare temperature and disks is an interesting new result, but does not appear to have a unique explanation and does not clarify whether or not reconnection occurs in star-disk field lines.

## 7.2. Magnetospheric truncation by a disk

Our second observational result is positive: the COUP flares provide the first direct evidence that the magnetic loops of powerful X-ray PMS flares can exceed the stellar corotation radius in diskfree stars, but do not exceed the corotation radius in disk stars (Figures 6-8). This finding is presented visually in Figure 12 which shows with realistic relative scaling the



largest inferred X-ray coronal extents for Class II and Class III stars. The high-order multipolar component of the magnetic field is expected to dominate at the stellar surface but fall off rapidly with height, leaving the dipolar component dominant at distances above a couple of stellar radii (Figure 15 in Donati et al. 2007, 2008). Figure 12 also shows schematically a compression and distortion of magnetic field lines by the accretion disk. More realistic field configurations with both accreting field lines and coronal loops are calculated by Jardine et al. (2006); Long et al. (2007).

For a T-Tauri star with radius of  $\sim 2 R_{\odot}$  and mass of  $\sim 0.5 M_{\odot}$ , the typical large flaring magnetic loops are roughly the same for the disk classes with  $L/R_{\star} \sim 5$ . But, due to the strong rotational acceleration after disks are gone, the corotation radii shrink so that loops formerly  $(L + R_{\star})/R_{cor} \lesssim 1$  during their disk phase are often  $1 \lesssim (L + R_{\star})/R_{cor} \lesssim 2$  during their diskfree phase. Table 1 shows that, as stars evolved from Class II to Class III phases, the average corotation radii decrease from  $R_{cor} \sim 7 R_{\star}$  to  $R_{cor} \sim 3 R_{\star}$  due to a shortening of the average rotation periods from  $P \sim 9$  day to  $P \sim 3$  day.

There are three independent supporting lines of evidence suggesting that long loop structures can be present in magnetically active stars when disks are not present.

1. Even the relatively inactive Sun has helmet-like X-ray streamers that reach up to  $\gtrsim 0.5 R_{\odot}$  above the photosphere. These occur in the subclass of the solar long decay events (LDEs). The analogies between solar LDEs and COUP bright X-ray flares are discussed in Paper I and in § 7.3 below.
2. Mullan et al. (2006) have carefully compared the loop sizes inferred from 106 flares studied with the *EUVE* satellite from 33 magnetically active main sequence stars, including members of RS CVn binaries and dMe stars. They find that stars with  $B - V < 1.4$  (hotter than M0) generally have loop lengths  $L/R_{\star} < 0.5$  while stars with  $B - V > 1.4$  (cooler than M0) often exhibit loop lengths  $L/R_{\star} \sim 1.0 - 1.5$ .
3. Radio VLBI studies have shown that magnetospheres likely extend several stellar radii in very active stars, filling with trans-relativistic electrons emitting gyrosynchrotron radiation. This is indicated by VLBI imaging of the RS CVn binary systems UX Ari HR 1099, and HR 5110 and the dMe stars YY Gem and UV Cet (Lang 1994; Alef et al. 1997; Benz et al. 1998; Franciosini et al. 1999; Ransom et al. 2002, 2003). While none of these systems showed loops larger than  $\sim 2$  times the photospheric radius, recent VLBI mapping of the nearby diskfree PMS binary system V773 Tau reveals radio structures extraordinarily far from the component stars. Their elongated magnetospheres resembling huge solar helmet streamers extending  $\simeq 20 R_{\star}$  yet are still anchored to the stellar surface (Massi et al. 2007).

As PMS stars lie at the extreme high-luminosity end of the  $10^{10}$  range of correlated X-ray and radio luminosities (the Benz-Güdel relation; see Figure 6 in Güdel 2002), it is reasonable that they also have the largest flare loop sizes. While the typical large coronal structures we find from COUP X-ray flares are  $\sim 5$  times the stellar radius, even larger structures are found for some cases. These magnetic structures must extend significantly beyond the corotation surface, implying that the loop magnetic fields are, at least temporarily, capable of withstanding both the thermal pressure of the confined hot gas and the effect of centrifugal forces (Jardine & Unruh 1999).

Our finding that the coronal structures in slower rotating Class II stars do not exceed their corotation surface agrees well with the T-Tauri coronal models of Jardine et al. (2006). Combining average COUP levels of X-ray emission with optical band measurements of multipolar surface magnetic fields and magnetic circumstellar disks, they calculate self-consistent 3-dimensional force-free field configurations. Their model emerges with a complicated combination of closed loops confining X-ray emitting plasma and open field lines available for accreting cool disk material or releasing a high velocity wind (see also Lovelace et al. 1995; Long et al. 2007). In the model of Jardine et al., X-ray coronal extents for diskfree PMS stars reach  $1.5 - 2.5 R_{cor}$ , precisely the range we find in the current work (Figures 6-8). The centrifugal stripping of the coronal outer parts proposed for rapidly rotating main-sequence stars, such as VXR 45 with a rotation period around 0.2 days (Jardine 2004), is apparently unimportant for relatively slow rotating T-Tauri stars.

We thus find that, while flare properties are mostly similar in Class II and Class III stars (§7.1), some differences are found. X-ray coronal structures on Class II stars are on average somewhat larger and are more likely to produce super-hot flares. This suggests the magnetic fields on accreting Class II stars may have distorted magnetic topologies as Jardine et al. (2006) predict. We discuss this further in §7.4.

### 7.3. Comparison with solar long decay events

It is reasonable to propose that the majority of the bright long X-ray flares detected from Orion T-Tauri stars are enhanced analogs of eruptive solar flare events classified as long decay events (LDEs, Kahler 1977). The *Skylab*, SMM and *Yohkoh* space observatories show these flares produce X-ray emitting arches and streamers with altitudes reaching up to several  $\times 10^{10}$  cm ( $\gtrsim 0.2 R_{\odot}$ , Švestka et al. 1995; Farnik et al. 1996; Švestka et al. 1997). The 24 Jan 1992 X-ray streamers, which reached up to  $L \gtrsim 0.5 R_{\odot}$  in altitude (Hiei 1994, 1997), are representative of magnetic structures emerging from solar LDEs (see inset in Figure 12). The X-ray lightcurves of LDE flares last from a few hours to a day, similar to the duration

of the COUP flares studied here (see Figure 14 in Paper I for two examples).

The origin of giant solar X-ray emitting arches and streamers is not well-understood. The most widely accepted model is that the impulsive flare near the solar surface ( $L \lesssim 10^{-2} R_{\odot}$ ) blows open the overlying large-scale magnetic field with subsequent reconnection of magnetic lines through a vertical current sheet. This model was developed over many years (e.g. Sturrock 1966; Kopp & Pneuman 1976; Forbes & Acton 1996) and is reviewed by Priest & Forbes (2002). Peak observed temperatures in giant solar arches and streamers are typically of several to  $\gtrsim 10$  MK with a wide range of plasma densities. For example, the 24 Jan 1992 event showed a relatively low density  $\lesssim 10^8 \text{ cm}^{-3}$  while the 15 Mar 1993 event showed densities  $\gtrsim 10^{10} \text{ cm}^{-3}$  (Getman & Livshitz 1999; Getman & Livshits 2000). Recall, however, that the peak luminosities and total energies of these solar flares are far below those we are studying in COUP stars, roughly  $E \sim 10^{30-31}$  ergs *vs.*  $E \sim 10^{35-37}$  ergs in the X-ray band integrated over the flare.

Confining a solar flare plasma with  $n_e \lesssim 10^8 \text{ cm}^{-3}$  and peak temperatures  $T \lesssim 10$  MK requires a local field strength exceeding 1 G. In the solar corona, the dipole component appears to become dominant at  $2.5 R_{\odot}$  (Luhmann et al. 1998) and the Sun’s magnetic dipole field, only  $\sim 1$  G at the surface, likely falls  $\lesssim 0.1$  G at this distance. Small-scale multipolar fields in active regions have surface strengths around 1000 G, but these quickly decay at large distances. Thus, the solar fields are too weak to confine X-ray emitting plasma at distances comparable to or exceeding the solar radius. The large-scale magnetic field of T-Tauri stars must thus be far stronger than in the Sun, as argued by Jardine et al. (2006) and others (§7.2, 7.4), and can sustain giant X-ray arches and streamers with sizes  $L/R_{\star} \sim 1 - 10$ . The recent reported discovery of the two solar-like radio-flaring streamers in the young binary system V773 Tau A reaching up the altitudes of  $> 20 R_{\star}$ , but apparently anchored at the surface of its host star (Massi et al. 2007), further strengthens the idea of the strong large-scale magnetic fields and giant X-ray flaring structures anchored at the stellar surface of T-Tauri stars.

We recall in this context our tentative finding (limited by small samples to a low statistical significance) that flares in accreting systems are systematically shorter than in other systems (§3.2). If this is true, it might be that high accretion may prevent very long lasting flares. In order to have relatively long-lasting flare events, magnetic stresses must build up over an extended time, storing magnetic energy accumulated from shearing and twisting of magnetic field lines. A similar process occurs in two-ribbon solar flares (Priest & Forbes 2002), although with much lower total energies. The magnetic field must be stable in order to store large stresses. It is possible that the process of accretion destabilizes the field, preventing the accumulation of magnetic stresses and forcing shorter flares.

We thus suggest that it is systematically shorter flare durations due to disrupted magnetic field configurations that may be responsible for the well-established reduction in time-integrated X-ray luminosities of accreting PMS stars compared to non-accreting stars. This interpretation is different from past explanations. Preibisch et al. (2005) suggested that X-ray emission from accretors is suppressed because it cannot arise in magnetic field lines which are mass-loaded with disk material. Jardine et al. (2006) argued that the outer magnetosphere of accretors is stripped by interaction with the disk. Gregory et al. (2007) proposed that soft X-ray emission is attenuated by dense material in accretion columns. The true cause of the reduced X-ray emission of Class II systems is thus still uncertain.

#### 7.4. Anomalous super-hot flares in accreting stars

We described in §5 and in Paper I a significant subset of COUP flares exhibiting peak temperatures exceeding 100 MK, some apparently exceeding 200 MK. These temperatures are hotter than any solar flare plasma, and hotter than nearly all reported stellar flares. The only comparable event we have identified is the  $T > 180$  MK plasma temperature in the 16 Dec 2005 flare in the RS CVn system II Peg using the hard X-ray detector (designed for gamma ray burst discovery) on board the *Swift* satellite (Osten et al. 2007). While the calibration of *Chandra* ACIS median energies to plasma temperatures above  $\sim 100$  MK is not precise, we argue in Appendix B of Paper I and the Appendix below that these events are indeed hotter than other flares in the sample.

While the super-hot flare phenomenon may have more than one cause, the clearest relation is to active accretion in lower-mass PMS stars. These are systems where the stellar radius is small and the stellar magnetosphere appears truncated by the inner disk at the corotation radius (§7.2). We show in §6 that these temperatures are too hot to be explained by standard dipolar fields rooted in the stellar surface. We speculate in § 7.1 that these conditions lead to a compression and intensification of field strength in the outer regions of the loop where the observed X-ray emission originates. This might lead to more violent reconnection and successful confinement of higher pressure plasmas. This interpretation qualitatively agrees with recent MHD computations of accretion funnels through PMS magnetospheres where distortion of initially dipolar field lines are predicted (Jardine et al. 2006; Bessolaz et al. 2008; Romanova et al. 2008). Other explanations such as reconnection in disk-derived fields (e.g., Hayashi et al. 1996) seem less attractive given the similarity of superhot and normal temperature flares in other properties (flare morphology and energetics).

## 8. Conclusions

We examine here empirical relationships between magnetic reconnection flares, protoplanetary disks and accretion. The current work provides detailed flare modeling of a much larger dataset than previously available: we consider 216 bright X-ray flares from 161 PMS stars observed during the 13-day COUP exposure of the Orion Nebula. Our sample is larger because, as described in Paper I, we use data analysis techniques that permit modeling of fainter flares than feasible with traditional parametric modeling of variable *Chandra* ACIS spectra. We thus have opportunity to uncover more subtle relationships between flaring, disks and accretion than were previously possible. The main results of our study are as follows:

1. Perhaps with the exception of the *Chandra* study of NGC 2264, where CTTS are seen to be more variable than WTTS (Flaccomio et al. 2006), past studies using smaller samples have not found differences in flare statistics or properties as a function of PMS evolutionary state or mass: accreting Class II systems appeared to flare like non-accreting Class III systems (e.g. Stelzer et al. 2000; Wolk et al. 2005; Favata et al. 2005; Stelzer et al. 2007). We confirm here that Class II and Class III systems produce X-ray flares with indistinguishable morphologies. Typical fast-rise slow-decay flares, composite step and double flares, and the unusual slow-rise flat-top flares are present in both classes. We have no clear evidence for distinctive flare types emerging from star-disk magnetic field lines. Accretion variations producing optical band variations are not associated with X-ray flares (Stassun et al. 2006). Accretion and magnetic flaring thus appear to be unrelated, even though the theory of PMS accretion involves magnetic truncation of disks and magnetic funneling of disk material onto the stellar surface. The COUP PMS flares are consistent with solar-type magnetic structures with both footpoints anchored in the stellar surface. Many may represent analogies of a much less powerful class of solar flares known as long duration events which produce giant coronal arches and X-ray streamers.

2. A distinct difference is found in the distribution of loop sizes. We find that X-ray coronal extents in fast rotating Class III stars sometimes exceeds the Keplerian corotation radius, whereas X-ray magnetospheres in Class II stars appear to be truncated at the inner edge of accreting protoplanetary disks. This directly supports theoretical models of magnetically mediated accretion, magnetic star-disk rotational coupling, and disk confinement of PMS magnetospheres.

3. A related, but statistically less secure, result is that flares from highly accreting Class II stars have somewhat shorter durations and weaker total X-ray energies than Class III flares. This might reflect the destabilization of magnetic arcades in accreting systems, and could account for the reduction of time-averaged X-ray luminosities in Class II compared to

Class III populations noted in previous studies.

4. A subclass of super-hot flares with peak plasma temperatures greater than 100 MK is noted for the first time. These are inconsistent with formation in normal dipolar magnetic loops attached to the stellar surface, and appear preferentially in accreting Class II systems. They may reflect compression and distortion of the large scale magnetospheric topology by star-disk magnetic interactions, as predicted by recent theoretical calculations.

We thank the anonymous referee for his time and useful comments that improved this work. The work was supported by the *Chandra* ACIS Team (G. Garmire, PI) through the SAO grant SV4-74018. G.M. acknowledges contribution from contract ASI-INAF I/088/06/0. This publication makes use of data products from the Two Micron All Sky Survey (a joint project of the University of Massachusetts and the Infrared Processing and Analysis Center/California Institute of Technology, funded by NASA and NSF), and archival data obtained with the *Spitzer Space Telescope* (operated by the Jet Propulsion Laboratory, California Institute of Technology under a contract with NASA).

## A. SUPER-HOT FLARES

It is difficult to accurately determine temperatures of thermal components  $\gtrsim 100$  MK from *Chandra*-ACIS spectra. To insure that the peak temperatures of  $T_{obs,pk} > 100$  MK do indeed describe the hottest flare plasmas observed in our sample, we describe here checks that have been performed beyond the analysis of the Appendix B of Paper I.

For each of the 216 COUP flares treated here, a spectrum has been extracted within the total time range  $[t_{flare1} - t_{flare2}]$ . Spectra were fitted with WABS  $\times$  MEKAL model (for compatibility with Getman et al. 2005a) with 0.3 times solar elemental abundances allowing both temperature and column density to be free parameters. The following confirmatory results are obtained. First, for the majority of the flares, the X-ray column densities obtained from the integrated flare spectral fits are in excellent agreement with the source column densities obtained from the full COUP observation by Getman et al. (2005a) that we used as fixed parameters during our flare analysis (see also Figure 16 in Paper I). Second, out of the 73 flares with peak flare temperatures  $T_{obs,pk} > 100$  MK, only 8 (11%) have their integrated flare spectral fits  $T_{flare} < 40$  MK, while 80% of the flares with  $T_{obs,pk} < 100$  MK have  $T_{flare} < 40$  MK (Figure 13). This confirms a distinct difference between super-hot and

ordinary flares. Third, high accreting stars<sup>10</sup> have the largest fraction of reported super-hot flares (9 out of 17 flares or 53%), three more flares from high accretors have their  $80 < T_{obs,pk} < 100$  MK. This confirms the discussion in §5 that high accretors preferentially exhibit super-hot flares.

Figure 14 further illustrates spectral differences between super-hot ( $T_{obs,pk} > 100$  MK) and ordinary flares. To avoid possible confounding effects of differing absorptions, flare histories and disk properties, we extract the spectrum within a brief 6 ks interval around the flare peak for all MIR disk sources in the narrow interval  $21.5 < \log(N_H) < 22$  cm<sup>-2</sup>. The figure compares combined flare peak spectra for sources with ordinary (panel *a*) and super-hot flares (panel *b*). Merging these spectra to improve the statistical accuracy, the best-fit model parameters of the composite 6 ks spectra are  $N_H = 4.8^{+0.5}_{-0.5} \times 10^{21}$  cm<sup>-2</sup> and  $kT = 5.5^{+1.0}_{-0.8}$  keV for the ordinary flares, and  $N_H = 6.6^{+0.6}_{-0.7} \times 10^{21}$  cm<sup>-2</sup> and  $kT = 15.2^{+12.1}_{-3.6}$  keV for the super-hot flares. The composite spectrum of super-hot flares can not be described by ordinary flare models (compare black and green lines in Figure 14*b*). This again demonstrates that super-hot flares are the hottest flares of our sample.

## REFERENCES

- Alef, W., Benz, A. O., & Guedel, M. 1997, *A&A*, 317, 707
- Argiroffi, C., Maggio, A., & Peres, G. 2007, *A&A*, 465, L5
- Arzner, K., Güdel, M., Briggs, K., Telleschi, A., & Audard, M. 2007, *A&A*, 468, 477
- Bally, J., Stark, A. A., Wilson, R. W., & Langer, W. D. 1987, *ApJ*, 312, L45
- Benz, A. O., Conway, J., & Gudel, M. 1998, *A&A*, 331, 596
- Bessolaz, N., Zanni, C., Ferreira, J., Keppens, R., & Bouvier, J. 2008, *A&A*, 478, 155
- Birk, G. T., Schwab, D., Wiechen, H., & Lesch, H. 2000, *A&A*, 358, 1027
- Bouvier, J., Alencar, S. H. P., Harries, T. J., Johns-Krull, C. M., & Romanova, M. M. 2007, *Protostars and Planets V*, 479
- Bouvier, J., & Appenzeller, I. 2007, *IAU Symposium*, 243,

---

<sup>10</sup>The twelve highly accreting stars with  $EW(CaII) < -2$  Å are COUP #11, 66, 141, 567, 579, 1044, 1045, 1080, 1096, 1335, 1409, and 1444.

- Browning, M. 2007, ArXiv e-prints, 712, arXiv:0712.1603
- Caramazza, M., Flaccomio, E., Micela, G., Reale, F., Wolk, S. J., & Feigelson, E. D. 2007, *A&A*, 471, 645
- Daou, A. G., Johns-Krull, C. M., & Valenti, J. A. 2006, *AJ*, 131, 520
- Donati, J.-F., et al. 2007, *MNRAS*, 380, 1297
- Donati, J. F., et al. 2008, ArXiv e-prints, 802, arXiv:0802.2052
- Drake, J. J., Testa, P., & Hartmann, L. 2005, *ApJ*, 627, L149
- Farnik et al. 1996, *Sol. Phys.*, 168, 331
- Favata, F., Flaccomio, E., Reale, F., Micela, G., Sciortino, S., Shang, H., Stassun, K. G., & Feigelson, E. D. 2005, *ApJS*, 160, 469
- Feigelson, E. D., & Montmerle, T. 1999, *ARA&A*, 37, 363
- Feigelson, E. D., et al. 2005, *ApJS*, 160, 379
- Feigelson, E., Townsley, L., Güdel, M., & Stassun, K. 2007, *Protostars and Planets V*, 313
- Flaccomio, E., Damiani, F., Micela, G., Sciortino, S., Harnden, F. R., Jr., Murray, S. S., & Wolk, S. J. 2003, *ApJ*, 582, 398
- Flaccomio, E., Micela, G., Sciortino, S., Feigelson, E. D., Herbst, W., Favata, F., Harnden, F. R., Jr., & Vrtillek, S. D. 2005, *ApJS*, 160, 450
- Flaccomio, E., Micela, G., & Sciortino, S. 2006, *A&A*, 455, 903
- Forbes, T. G., & Acton, L. W. 1996, *ApJ*, 459, 330
- Franciosini, E., Massi, M., Paredes, J. M., & Estalella, R. 1999, *A&A*, 341, 595
- Franciosini, E., et al. 2007, *A&A*, 468, 485
- Getman, K. V., & Livshitz, M. A. 1999, *Astronomy Reports*, 43, 615
- Getman, K. V., & Livshits, M. A. 2000, *Astronomy Reports*, 44, 255
- Getman, K. V., Flaccomio, E., Broos, P. S. and 21 co-authours 2005, *ApJS*, 160, 319
- Getman, K. V., Feigelson, E. D., Townsley, L., Broos, P., Garmire, G., & Tsujimoto, M. 2006, *ApJS*, 163, 306



- Getman, K. V., Feigelson, E. D., Broos, P. S., Micela, G., & Garmire, G. P. 2008, *ApJ*, in press (Paper I)
- Getman, K. V., Feigelson, E. D., Garmire, G., Broos, P., & Wang, J. 2007, *ApJ*, 654, 316
- Gregory, S. G., Jardine, M., Simpson, I., & Donati, J.-F. 2006a, *MNRAS*, 371, 999
- Gregory, S. G., Jardine, M., Cameron, A. C., & Donati, J.-F. 2006b, *MNRAS*, 373, 827
- Gregory, S. G., Wood, K., & Jardine, M. 2007, *MNRAS*, 379, L35
- Grosso, N., et al. 2005, *ApJS*, 160, 530
- Güdel, M. 2002, *ARA&A*, 40, 217
- Güdel, M. 2004, *A&A Rev.*, 12, 71
- Güdel, M., et al. 2007, *A&A*, 468, 353
- Güdel, M., & Telleschi, A. 2007, *A&A*, 474, L25
- Hartmann, L. 1998, *Accretion processes in star formation* / Lee Hartmann. Cambridge, UK ; New York : Cambridge University Press
- Hartmann, L., Megeath, S. T., Allen, L., Luhman, K., Calvet, N., D’Alessio, P., Franco-Hernandez, R., & Fazio, G. 2005, *ApJ*, 629, 881
- Hayashi, M. R., Shibata, K., & Matsumoto, R. 1996, *ApJ*, 468, L37
- Herbst, W., Bailer-Jones, C. A. L., Mundt, R., Meisenheimer, K., & Wackermann, R. 2002, *A&A*, 396, 513
- Hiei, E. 1994, *IAU Colloq. 144: Solar Coronal Structures*, 163
- Hiei, E. 1997, *Memorie della Societa Astronomica Italiana*, 68, 491
- Hillenbrand, L. A. 1997, *AJ*, 113, 1733
- Huenemoerder, D. P., Kastner, J. H., Testa, P., Schulz, N. S., & Weintraub, D. A. 2007, *ApJ*, 671, 592
- Imanishi, K., Nakajima, H., Tsujimoto, M., Koyama, K., & Tsuboi, Y. 2003, *PASJ*, 55, 653
- Isobe, H., Shibata, K., Yokoyama, T., & Imanishi, K. 2003, *PASJ*, 55, 967
- Jardine, M., & Unruh, Y. C. 1999, *A&A*, 346, 883

- Jardine, M. 2004, *A&A*, 414, L5
- Jardine, M., Cameron, A. C., Donati, J.-F., Gregory, S. G., & Wood, K. 2006, *MNRAS*, 367, 917
- Johns-Krull, C. M., Valenti, J. A., Hatzes, A. P., & Kanaan, A. 1999, *ApJ*, 510, L41
- Johns-Krull, C. M. 2007, *ApJ*, 664, 975
- Kahler, S. 1977, *ApJ*, 214, 891
- Kastner, J. H., Huenemoerder, D. P., Schulz, N. S., Canizares, C. R., & Weintraub, D. A. 2002, *ApJ*, 567, 434
- Kelly, B. C. 2007, *ApJ*, 665, 1489
- Kopp, R. A., & Pneuman, G. W. 1976, *Sol. Phys.*, 50, 85
- Koyama, K., Hamaguchi, K., Ueno, S., Kobayashi, N., & Feigelson, E. D. 1996, *PASJ*, 48, L87
- Lang, K. R. 1994, *ApJS*, 90, 753
- Long, M., Romanova, M. M., & Lovelace, R. V. E. 2005, *ApJ*, 634, 1214
- Long, M., Romanova, M. M., & Lovelace, R. V. E. 2007, *MNRAS*, 374, 436
- Lovelace, R. V. E., Romanova, M. M., & Bisnovatyi-Kogan, G. S. 1995, *MNRAS*, 275, 244
- Luhmann, J. G., Gosling, J. T., Hoeksema, J. T., & Zhao, X. 1998, *J. Geophys. Res.*, 103, 6585
- Maggio, A., Pallavicini, R., Reale, F., & Tagliaferri, G. 2000, *A&A*, 356, 627
- Maggio, A., Flaccomio, E., Favata, F., Micela, G., Sciortino, S., Feigelson, E. D., & Getman, K. V. 2007, *ApJ*, 660, 1462
- Mathis, J. S. 1990, *The Evolution of the Interstellar Medium*, 12, 63
- Massi, M., et al. 2007, *ArXiv e-prints*, 712, arXiv:0712.0718
- Montmerle, T., Grosso, N., Tsuboi, Y., & Koyama, K. 2000, *ApJ*, 532, 1097
- Mullan, D. J., Mathioudakis, M., Bloomfield, D. S., & Christian, D. J. 2006, *ApJS*, 164, 173

- Osten, R. A., Drake, S., Tueller, J., Cummings, J., Perri, M., Moretti, A., & Covino, S. 2007, *ApJ*, 654, 1052
- Preibisch, T., et al. 2005b, *ApJS*, 160, 401
- Priest, E. R., & Forbes, T. G. 2002, *A&A Rev.*, 10, 313
- Prisinzano, L., et al. 2007, *ArXiv e-prints*, 712, arXiv:0712.2975
- Ransom, R. R., Bartel, N., Bietenholz, M. F., Lebach, D. E., Ratner, M. I., Shapiro, I. I., & Lestrade, J.-F. 2002, *ApJ*, 572, 487
- Ransom, R. R., Bartel, N., Bietenholz, M. F., Ratner, M. I., Lebach, D. E., Shapiro, I. I., & Lestrade, J.-F. 2003, *ApJ*, 587, 390
- Reale, F., Betta, R., Peres, G., Serio, S., & McTiernan, J. 1997, *A&A*, 325, 782
- Reale, F. 2002, *Stellar Coronae in the Chandra and XMM-NEWTON Era*, 277, 103
- Reale, F. 2007, *A&A*, 471, 271
- Rebull, L. M., Stauffer, J. R., Megeath, S. T., Hora, J. L., & Hartmann, L. 2006, *ApJ*, 646, 297
- Romanova, M. M., Kulkarni, A. K., & Lovelace, R. V. E. 2008, *ApJ*, 673, L171
- Schmitt, J. H. M. M., Robrade, J., Ness, J.-U., Favata, F., & Stelzer, B. 2005, *A&A*, 432, L35
- Shu, F., Najita, J., Ostriker, E., Wilkin, F., Ruden, S., & Lizano, S. 1994, *ApJ*, 429, 781
- Shu, F. H., Shang, H., Glassgold, A. E., & Lee, T. 1997, *Science*, 277, 1475
- Siess, L., Dufour, E., & Forestini, M. 2000, *A&A*, 358, 593
- Simon, T., & Dahm, S. E. 2005, *ApJ*, 618, 795
- Stassun, K. G., van den Berg, M., Feigelson, E., & Flaccomio, E. 2006, *ApJ*, 649, 914
- Stelzer, B., Neuhauser, R., & Hambaryan, V. 2000, *A&A*, 356, 949
- Stelzer, B., Flaccomio, E., Briggs, K., Micela, G., Scelsi, L., Audard, M., Pillitteri, I., Güdel, M. 2007, *A&A*, 468, 463
- Sturrock, P. A. 1966, *Nature*, 211, 695

- Švestka, Z., Fárník, F., Hudson, H. S., Uchida, Y., Hick, P., & Lemen, J. R. 1995, *Sol. Phys.*, 161, 331
- Svestka, Z., Farnik, F., Hick, P., Hudson, H. S., & Uchida, Y. 1997, *Sol. Phys.*, 176, 355
- Symington, N. H., Harries, T. J., Kurosawa, R., & Naylor, T. 2005, *MNRAS*, 358, 977
- Tsuboi, Y., Koyama, K., Murakami, H., Hayashi, M., Skinner, S., & Ueno, S. 1998, *ApJ*, 503, 894
- Vuong, M. H., Montmerle, T., Grosso, N., Feigelson, E. D., Verstraete, L., & Ozawa, H. 2003, *A&A*, 408, 581
- Wolk, S. J., Harnden, F. R., Jr., Flaccomio, E., Micela, G., Favata, F., Shang, H., & Feigelson, E. D. 2005, *ApJS*, 160, 423
- Yang, H., Johns-Krull, C. M., & Valenti, J. A. 2007, *AJ*, 133, 73

Table 1. Summary of Stellar Properties

Quantity (1)	N (2)	Flag (3)	Min (4)	Max (5)	Median (6)	Mean $\pm$ SD (7)	$P_{KS}$ (8)
X-ray Absorbing Column Density ( $\text{cm}^{-2}$ )							
$\log(NH)$ (all available)	161	s	20.0	22.8	21.6	$21.5 \pm 0.6$	...
$\log(NH_{NIRdisk})$ (NIR inner disk)	56	s	20.0	22.6	21.7	$21.6 \pm 0.6$	...
$\log(NH_{noNIRdisk})$ (no NIR inner disk)	84	s	20.0	22.3	21.5	$21.4 \pm 0.6$	0.09
$\log(NH_{MIRdisk})$ (MIR disk)	62	s	20.0	22.8	21.8	$21.7 \pm 0.6$	...
$\log(NH_{noMIRdisk})$ (no MIR disk)	50	s	20.0	22.5	21.3	$21.3 \pm 0.6$	0.02
Stellar Mass ( $M_{\odot}$ )							
$M$ (all available)	128	s	0.2	5.0	0.7	$1.0 \pm 0.9$	...
$M_{NIRdisk}$ (NIR inner disk)	42	s	0.2	5.0	0.7	$1.1 \pm 1.1$	...
$M_{noNIRdisk}$ (no NIR inner disk)	72	s	0.2	2.3	0.6	$1.0 \pm 0.8$	0.1
$M_{MIRdisk}$ (MIR disk)	44	s	0.2	5.0	0.7	$1.1 \pm 0.9$	...
$M_{noMIRdisk}$ (no MIR disk)	42	s	0.2	2.3	0.6	$1.0 \pm 0.9$	0.4
Stellar Radius ( $10^{10}$ cm)							
$R_{\star}$ (all available)	130	s	4	90	18	$20 \pm 12$	...
$R_{\star,NIRdisk}$ (NIR inner disk)	44	s	5	90	16	$19 \pm 15$	...
$R_{\star,noNIRdisk}$ (no NIR inner disk)	72	s	4	58	18	$21 \pm 11$	0.5
$R_{\star,MIRdisk}$ (MIR disk)	45	s	4	32	14	$17 \pm 7$	...
$R_{\star,noMIRdisk}$ (no MIR disk)	43	s	10	58	17	$22 \pm 12$	0.3
Stellar Rotational Period (day)							
$P$ (all available)	79	s	1.1	19.5	6.5	$6.7 \pm 3.9$	...
$P_{NIRdisk}$ (NIR inner disk)	20	s	1.4	14.4	8.5	$7.7 \pm 2.8$	...
$P_{noNIRdisk}$ (no NIR inner disk)	48	s	1.1	19.5	6.3	$6.3 \pm 4.2$	0.06
$P_{MIRdisk}$ (MIR disk)	24	s	5.2	14.4	9.0	$8.8 \pm 1.9$	...
$P_{noMIRdisk}$ (no MIR disk)	35	s	1.1	19.5	3.5	$5.5 \pm 4.6$	<0.0001

Table 1—Continued

Quantity (1)	N (2)	Flag (3)	Min (4)	Max (5)	Median (6)	Mean $\pm$ SD (7)	$P_{KS}$ (8)
Keplerian Co-rotation Radius ( $10^{10}$ cm)							
$R_{cor}$ (all available)	67	s	22	270	85	$90 \pm 47$	...
$R_{cor,NIRdisk}$ (NIR inner disk)	14	s	39	180	120	$107 \pm 39$	...
$R_{cor,noNIRdisk}$ (no NIR inner disk)	44	s	22	270	84	$87 \pm 50$	0.03
$R_{cor,MIRdisk}$ (MIR disk)	21	s	54	180	98	$108 \pm 33$	...
$R_{cor,noMIRdisk}$ (no MIR disk)	31	s	22	270	76	$83 \pm 55$	0.007
Ratio of Co-rotation Radius to Stellar Radius							
$R_{cor}/R_{\star}$ (all available)	67	s	1.4	20.9	5.1	$5.7 \pm 3.9$	...
$(R_{cor}/R_{\star})_{NIRdisk}$ (NIR inner disk)	14	s	3.0	16.3	7.4	$8.1 \pm 3.6$	...
$(R_{cor}/R_{\star})_{noNIRdisk}$ (no NIR inner disk)	44	s	1.5	20.9	4.2	$5.3 \pm 4.0$	0.01
$(R_{cor}/R_{\star})_{MIRdisk}$ (MIR disk)	21	s	3.0	17.2	7.2	$8.1 \pm 3.6$	...
$(R_{cor}/R_{\star})_{noMIRdisk}$ (no MIR disk)	31	s	1.4	13.6	3.2	$4.0 \pm 2.7$	<0.0001

Note. — Columns 1: Quantity name. Column 2: Number of flares (Flag=f, see Column 3) or sources (Flag=s) in a sample. Column 3: Flag indicates if this is a flare (f) or source (s) sample. Columns 4-6: Min, max, median values for a considered quantity's distribution. Column 7: Mean and standard deviation for a considered quantity's distribution. Column 8: K-S probability for the assumption that distributions of a considered quantity in disk and diskfree stars are drawn from the same underlying distribution.

Table 2. Summary of Flare Properties

Quantity (1)	N (2)	Flag (3)	Min (4)	Max (5)	Median (6)	Mean $\pm$ SD (7)	$P_{KS}$ (8)
Peak Flare Luminosity (erg s $^{-1}$ )							
$\log(L_{X,pk})$ (all available)	216	f	30.45	32.92	31.33	$31.38 \pm 0.51$	...
$\log(L_{X,pk,NIRdisk})$ (NIR inner disk)	78	f	30.44	32.51	31.35	$31.36 \pm 0.46$	...
$\log(L_{X,pk,noNIRdisk})$ (no NIR inner disk)	106	f	30.53	32.92	31.38	$31.41 \pm 0.52$	0.9
$\log(L_{X,pk,MIRdisk})$ (MIR disk)	89	f	30.49	32.51	31.27	$31.32 \pm 0.44$	...
$\log(L_{X,pk,noMIRdisk})$ (no MIR disk)	60	f	30.57	32.77	31.38	$31.40 \pm 0.53$	0.4
Peak Flare Temperature (MK)							
$T_{pk}$ (all available)	216	f	19	700	63	$141 \pm 178$	...
$T_{pk,NIRdisk}$ (NIR inner disk)	78	f	23	700	73	$170 \pm 209$	...
$T_{pk,noNIRdisk}$ (no NIR inner disk)	106	f	19	700	59	$123 \pm 153$	0.5
$T_{pk,MIRdisk}$ (MIR disk)	89	f	19	700	84	$181 \pm 209$	...
$T_{pk,noMIRdisk}$ (no MIR disk)	60	f	20	600	57	$102 \pm 114$	0.009
Inferred Loop Size (10 $^{10}$ cm)							
$L$ (all available)	175	f	0.4	510	43	$64 \pm 70$	...
$L_{NIRdisk}$ (NIR inner disk)	59	f	4	420	43	$60 \pm 63$	...
$L_{noNIRdisk}$ (no NIR inner disk)	89	f	6	510	43	$67 \pm 71$	0.8
$L_{MIRdisk}$ (MIR disk)	68	f	4	510	56	$79 \pm 86$	...
$L_{noMIRdisk}$ (no MIR disk)	54	f	0.4	300	37	$54 \pm 55$	0.12
Ratio of Loop Size to Stellar Radius							
$L/R_{\star}$ (all available)	147	f	0.03	45	2.4	$4.4 \pm 7.3$	...
$(L/R_{\star})_{NIRdisk}$ (NIR inner disk)	48	f	0.14	33	2.5	$4.0 \pm 5.1$	...
$(L/R_{\star})_{noNIRdisk}$ (no NIR inner disk)	81	f	0.2	46	2.4	$4.6 \pm 7.9$	0.5
$(L/R_{\star})_{MIRdisk}$ (MIR disk)	52	f	0.4	46	3.0	$5.9 \pm 8.2$	...
$(L/R_{\star})_{noMIRdisk}$ (no MIR disk)	47	f	0.03	29	1.8	$2.9 \pm 4.4$	0.009

Table 2—Continued

Quantity (1)	N (2)	Flag (3)	Min (4)	Max (5)	Median (6)	Mean±SD (7)	$P_{KS}$ (8)
Ratio of Loop Size to Co-rotation Radius							
$L/R_{cor}$ (all available)	81	f	0.007	5.4	0.51	$0.73 \pm 0.76$	...
$(L/R_{cor})_{NIRdisk}$ (NIR inner disk)	18	f	0.08	1.3	0.51	$0.54 \pm 0.30$	...
$(L/R_{cor})_{noNIRdisk}$ (no NIR inner disk)	51	f	0.05	5.4	0.51	$0.82 \pm 0.88$	0.15
$(L/R_{cor})_{MIRdisk}$ (MIR disk)	30	f	0.07	5.4	0.45	$0.66 \pm 0.94$	...
$(L/R_{cor})_{noMIRdisk}$ (no MIR disk)	33	f	0.007	2.4	0.69	$0.78 \pm 0.66$	0.19
Ratio of Loop Size plus Stellar Radius to Co-rotation Radius							
$(L + R_{\star})/R_{cor}$ (all available)	81	f	0.16	5.5	0.72	$0.98 \pm 0.80$	...
$((L + R_{\star})/R_{cor})_{NIRdisk}$ (NIR inner disk)	18	f	0.28	1.5	0.66	$0.69 \pm 0.32$	...
$((L + R_{\star})/R_{cor})_{noNIRdisk}$ (no NIR inner disk)	51	f	0.16	5.5	0.88	$1.11 \pm 0.90$	0.08
$((L + R_{\star})/R_{cor})_{MIRdisk}$ (MIR disk)	30	f	0.24	5.49	0.62	$0.81 \pm 0.94$	...
$((L + R_{\star})/R_{cor})_{noMIRdisk}$ (no MIR disk)	33	f	0.18	3.11	0.98	$1.14 \pm 0.75$	0.01

Note. — Columns 1: Quantity name. In case of loop sizes, summary is provided for a distribution of a mean value of the inferred loop size ranges. Column 2: Number of flares (Flag=f, see Column 3) or sources (Flag=s) in a sample. Column 3: Flag indicates if this is a flare (f) or source (s) sample. Columns 4-6: Min, max, median values for a considered quantity's distribution. Column 7: Mean and standard deviation for a considered quantity's distribution. Column 8: K-S probability for the assumption that distributions of a considered quantity in disky and diskfree stars are drawn from the same underlying distribution.



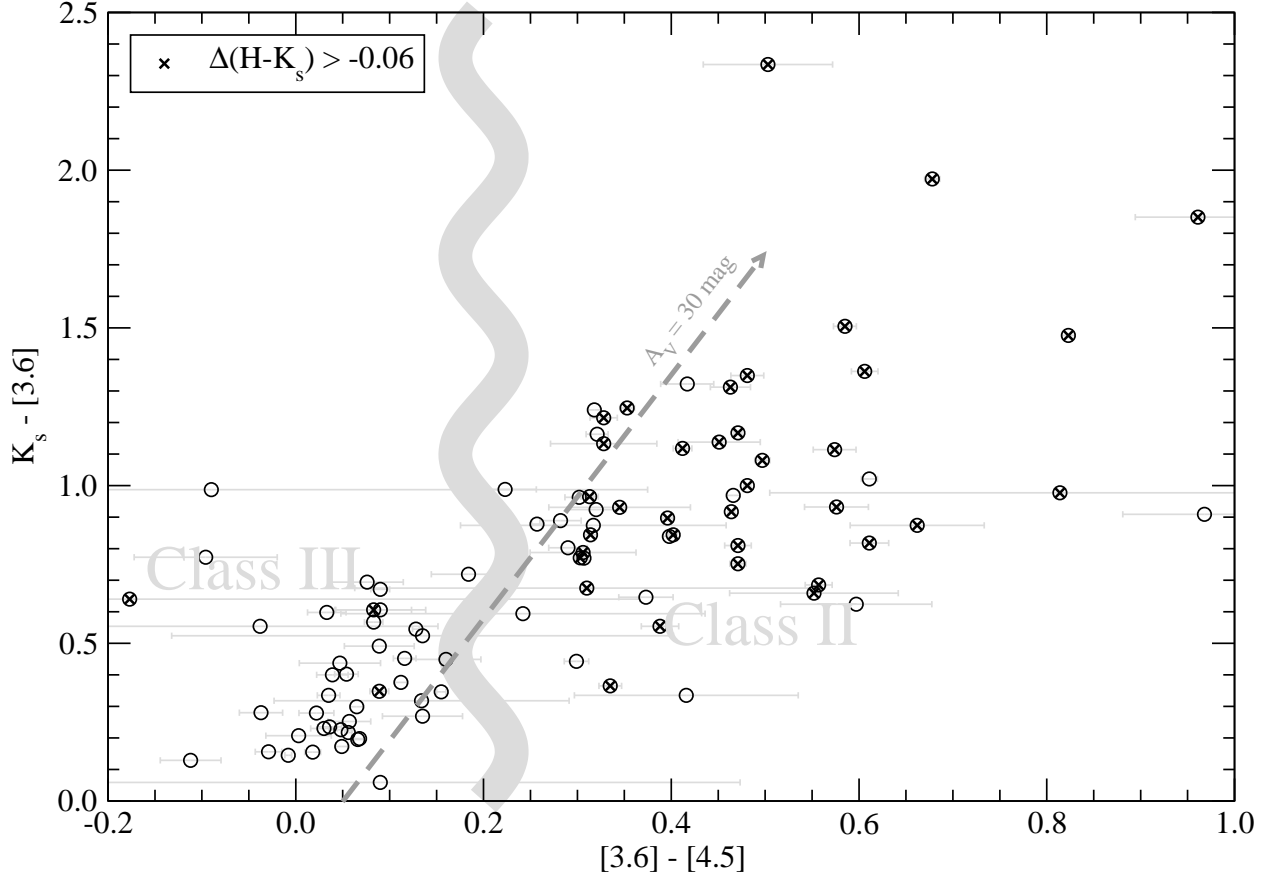


Fig. 1.— Disk indicators  $K_s - [3.6]$  vs.  $[3.6] - [4.5]$  color-color diagram for 98 COUP sources with available infrared photometry. For 59 sources  $\Delta(H - K_s) < -0.06$  mag indicating no inner disk, while for 39 sources (marked by  $\times$ )  $\Delta(H - K_s) > -0.06$  mag indicating an inner disk. Reddening vector of  $A_V \sim 30$  mag is shown as the grey arrow. The grey serpent line roughly discriminates between stars with and without a MIR excess from a circumstellar disk. Typical errors on  $K_s - [3.6]$  are 0.02 mag, while errors on  $[3.6] - [4.5]$  are shown as grey bars.

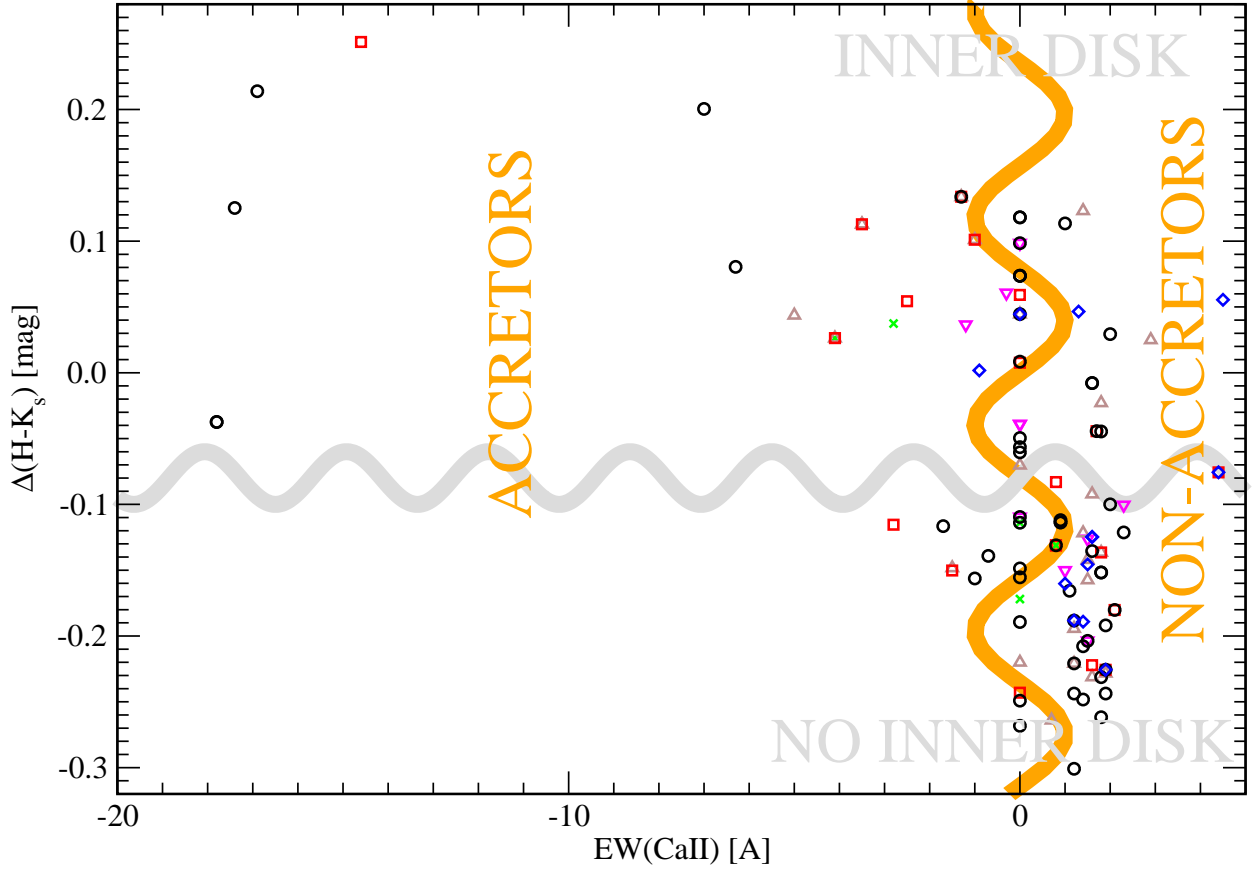


Fig. 2.— Inner disk indicator  $\Delta(H - K_s)$  vs. accretion indicator from the 8542 Å Ca II line for 128 flares on 96 COUP stars with available data. Symbols represent flare morphologies: 57 “typical” flares (black circles); 21 “step” flares (red boxes); 12 “slow-rise-and/or-top-flat” flares (blue diamonds); 23 “incomplete” flares (brown triangles); 5 “double” flares (green ×); and 10 “other” flares (magenta triangles). The grey serpent line roughly discriminates between stars with and without inner disk. The orange serpent line very roughly discriminates between stars with and without accretion.

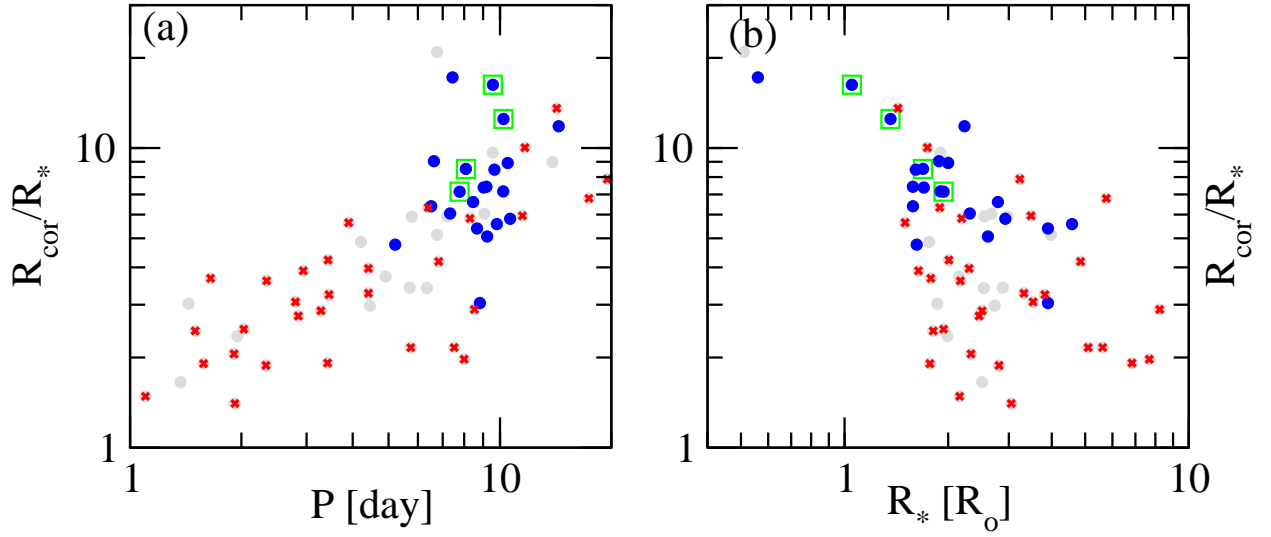


Fig. 3.— Confirmation of PMS disk-rotation relationship: (a) Keplerian corotation radius scaled to stellar radius *vs.* stellar rotational period; and (b) Keplerian corotation radius scaled to stellar radius versus stellar radius. Panels present results for all stars with available stellar properties (67 out of 161). Symbols indicate subsamples: stars with MIR excess disk stars (blue circles), without MIR disks (red crosses), uncertain disks (grey circles), and highly accreting stars with  $EW(CaII) < -2 \text{ \AA}$  (green boxes).

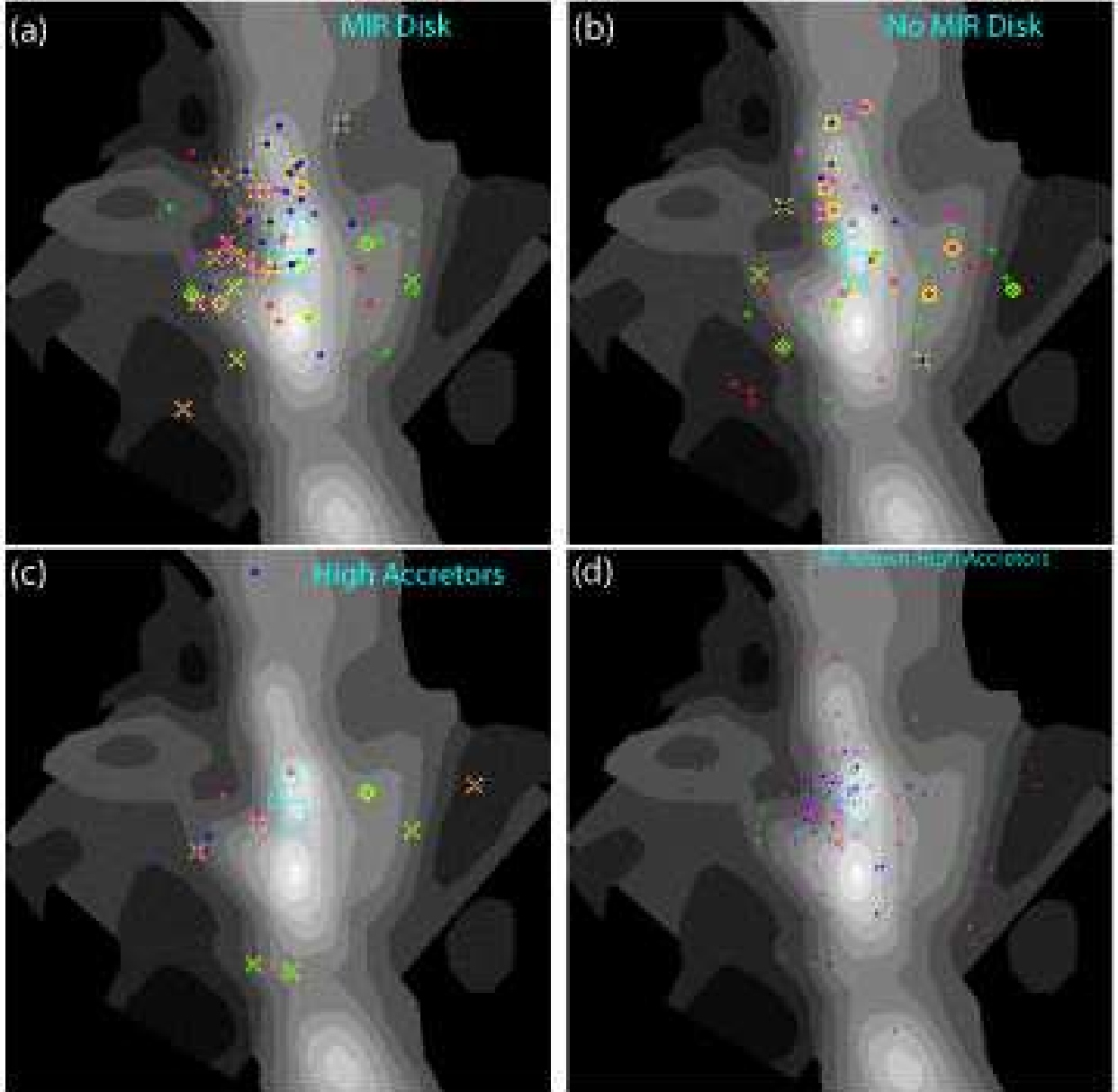


Fig. 4.— Locations of subsamples of X-ray bright flaring COUP stars plotted on the map of the OMC derived from the velocity-integrated intensity of  $^{13}\text{CO}$  (Bally et al. 1987). Symbols are coded by their X-ray absorption:  $\log(N_H) < 21 \text{ cm}^{-2}$  (red),  $21 < \log(N_H) < 21.5 \text{ cm}^{-2}$  (green),  $21.5 < \log(N_H) < 22 \text{ cm}^{-2}$  (magenta), and  $22 < \log(N_H) < 22.8 \text{ cm}^{-2}$  (blue). Stars with masses  $M > 2 M_\odot$  are outlined by yellow diamonds; stars harboring super-hot ( $T_{\text{obs},pk} > 100 \text{ MK}$ ) flares are labelled by yellow  $\times$ . Two small cyan boxes indicate BN/KL and OMC1-S regions (Grosso et al. 2005), and the cyan circle marks  $\theta^1 \text{ Ori C}$  at the center of the Orion Nebula Cluster.

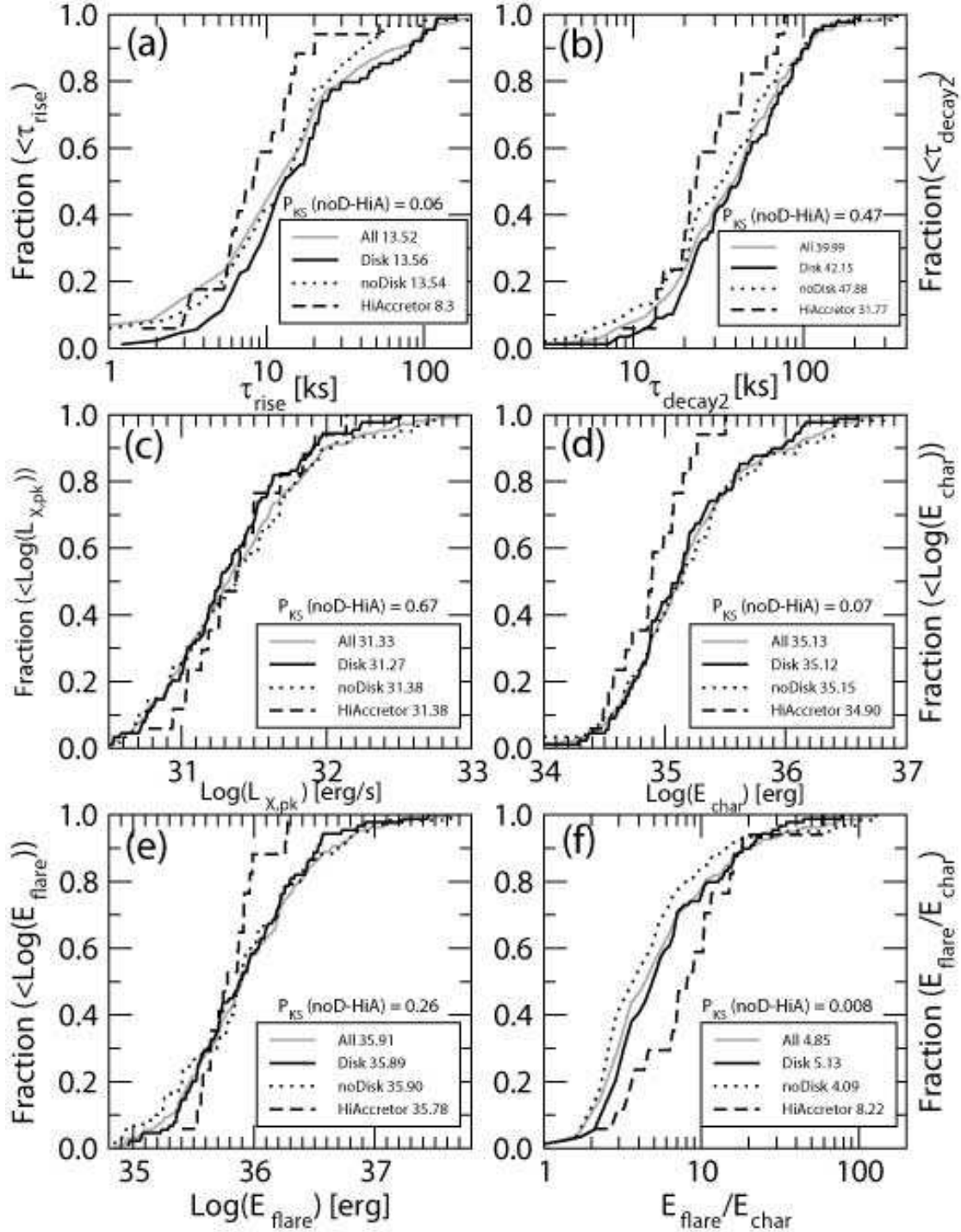


Fig. 5.— Cumulative distributions of flare rise (a) and decay (b) timescales; X-ray flare peak luminosity (c); energy from the “characteristic” state within flare duration time; (d); flare energy (e); and ratio of energies in flare and “characteristic” states (f). Line types indicate samples: all 216 flares (grey), 89 flares from MIR disk stars (solid black), 60 diskfree stars (dotted black), and 17 high-accretor stars (dashed black). Legends indicate median values, and KS test probability compare diskfree and high-accretor stars.

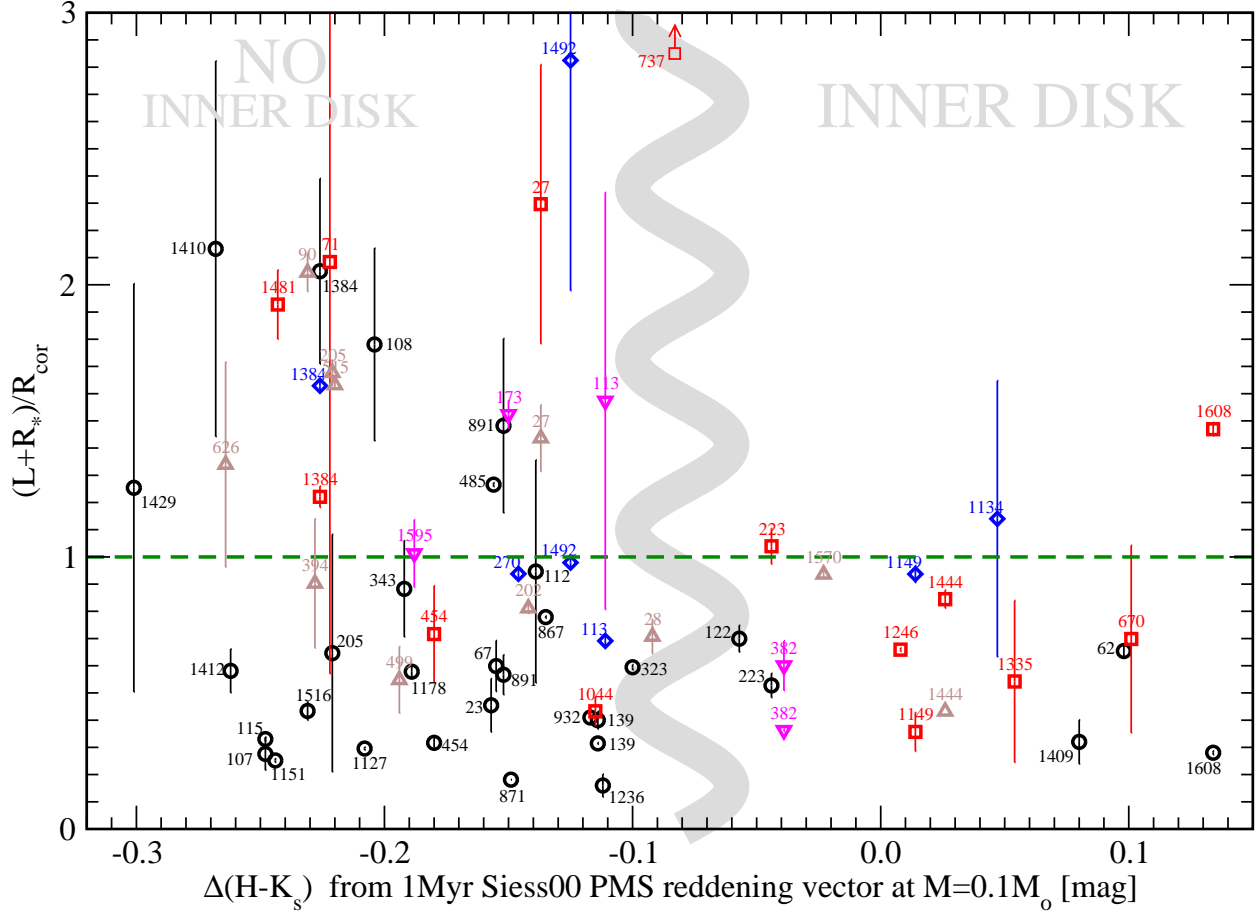


Fig. 6.— Inferred sizes of coronal flaring structures scaled to stellar corotation radii *vs.*  $K_s$ -excess inner disk indicator. Results are shown for 69 flares from 56 COUP stars with available data. Flares are labelled by corresponding COUP source numbers. Symbols distinguish flare morphologies: 32 “typical” flares (black circles); 14 “step” flares (red boxes); 7 “slow-rise-and/or-top-flat” flares (blue diamonds); 11 “incomplete” flares (brown triangles); and 5 “other” flares (magenta triangles). The grey serpent line roughly discriminates between stars with and without inner disks. The vertical bars represent boundaries of the inferred loop size ranges (Paper I) with symbols positioned at the mean of those ranges.

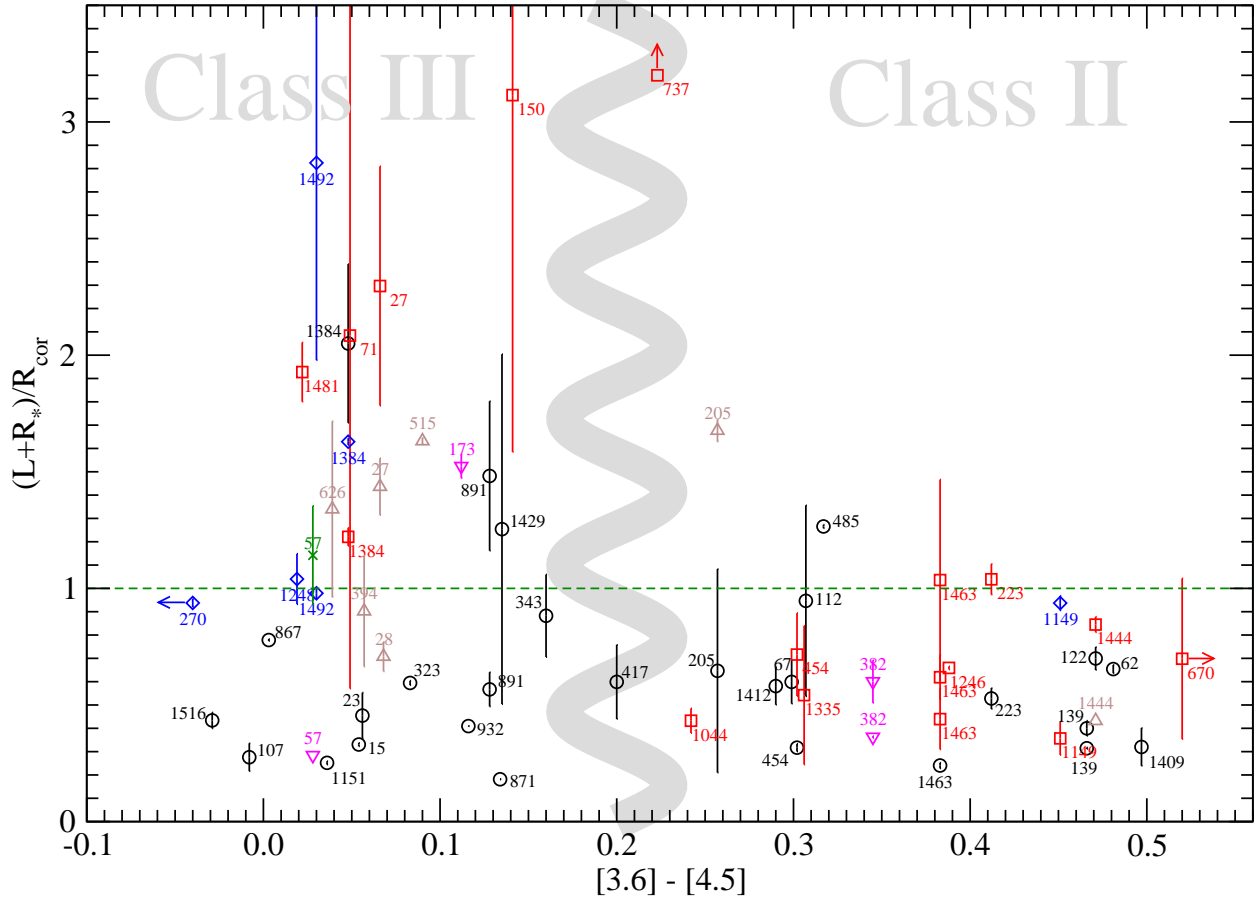


Fig. 7.— Inferred sizes of coronal flaring structures scaled to stellar corotation radii *vs.*  $[3.6] - [4.5]$  MIR disk indicator. Results are shown for 63 flares from 47 COUP stars with available data. See Figure 6 for symbols.

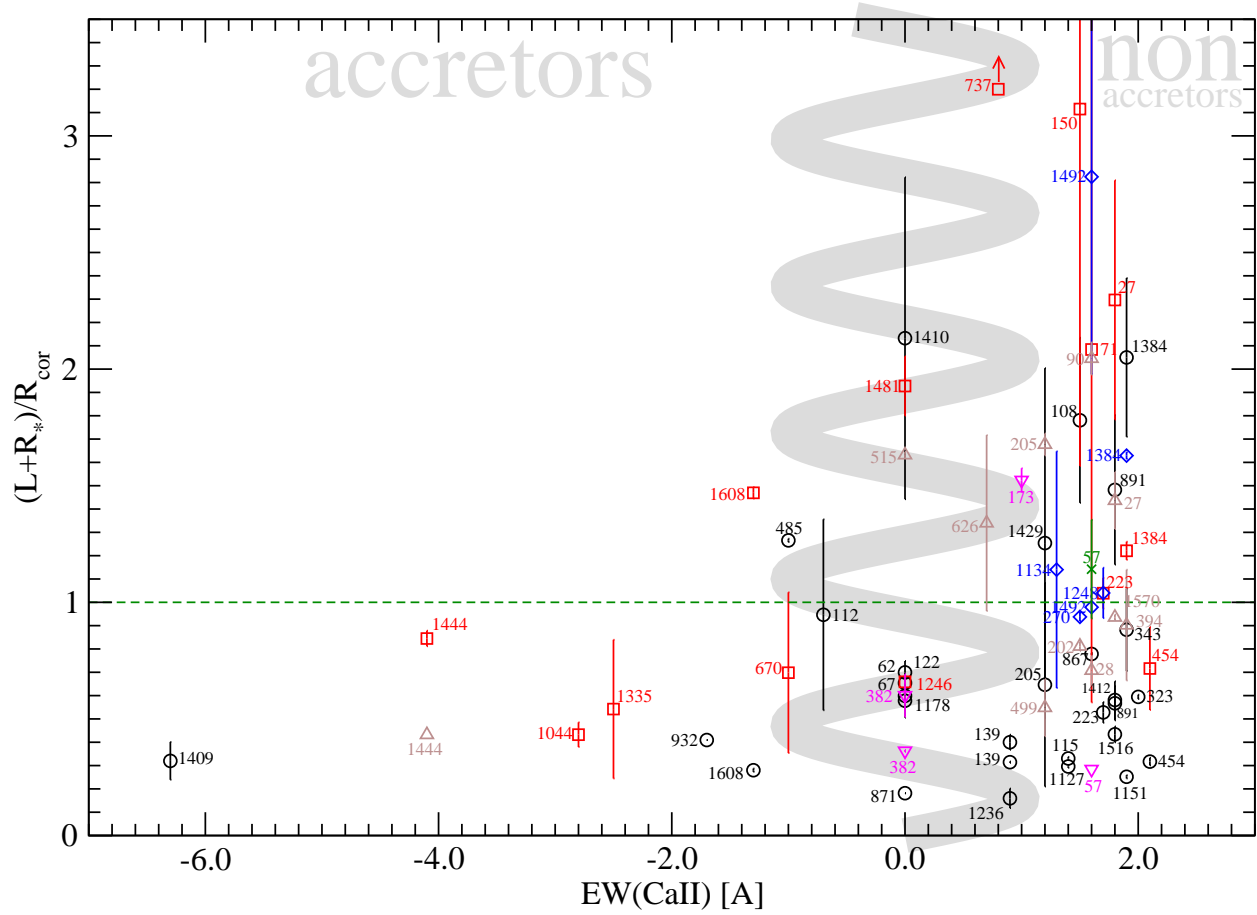


Fig. 8.— Inferred sizes of coronal flaring structures scaled to stellar corotation radii *vs.* 8542 Å Ca II line accretion indicator. Results are shown for 66 flares from 53 COUP stars with available information data. The grey serpent line roughly discriminates between stars with and without accretion. See Figure 6 for symbols.



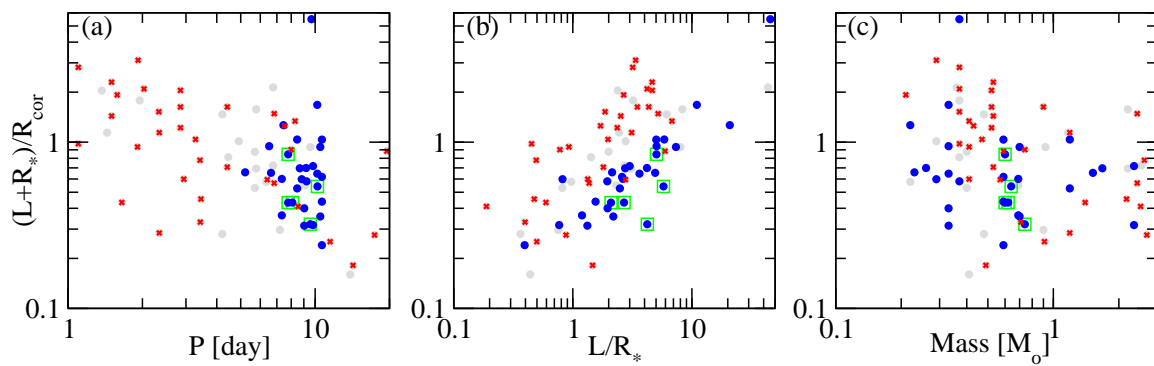


Fig. 9.— Coronal extents of analyzed flaring structures *vs.*: (a) stellar rotational period; (b) loop size normalized to stellar radius; and (c) stellar mass. See Figure 3 for symbols.

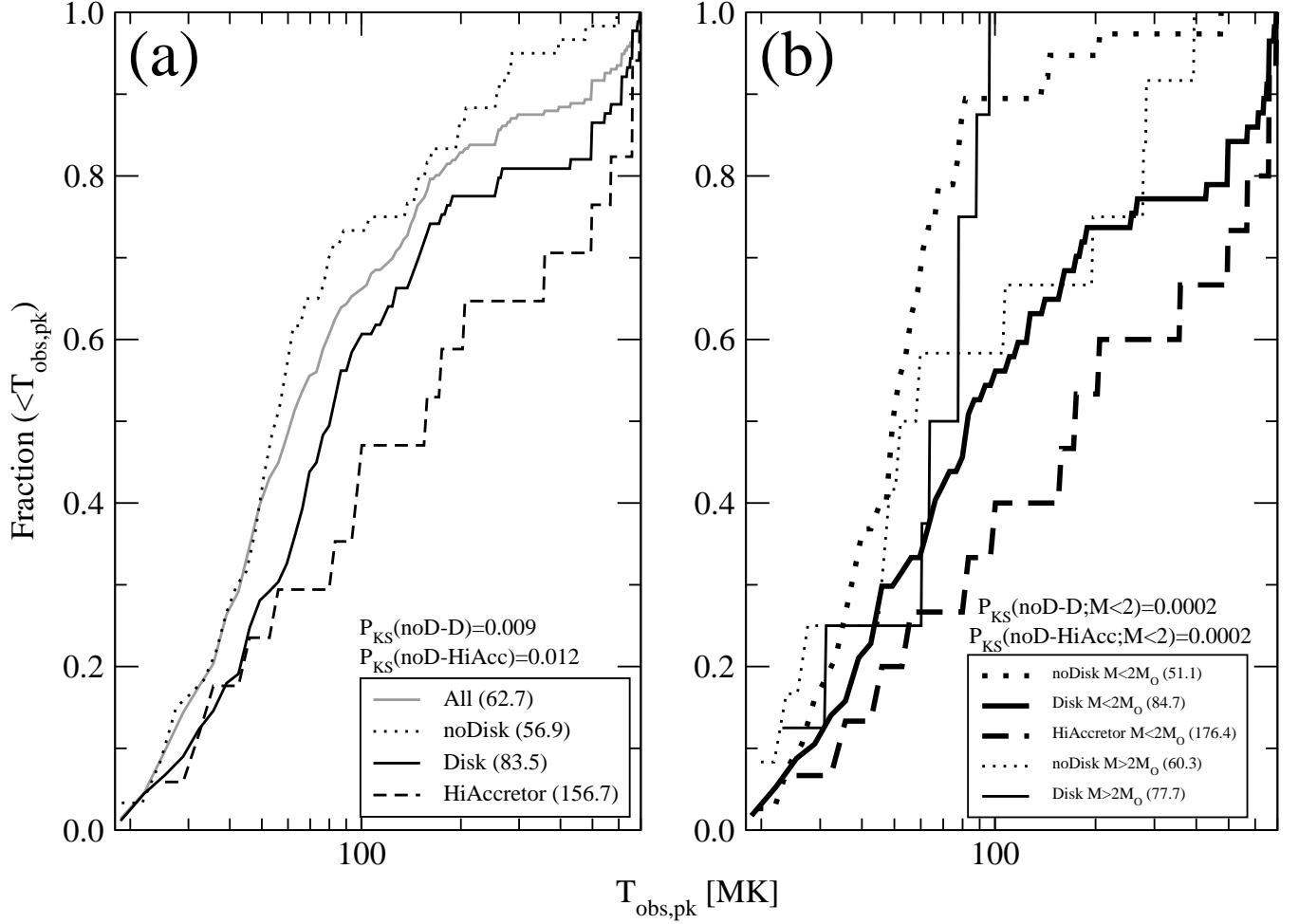


Fig. 10.— (a) Cumulative distributions of flare peak temperature for all 216 flares (grey line), 89 flares from MIR disk stars (solid black), 60 from diskfree stars (dotted), and 17 from high-accretors (dashed). (b) Mass-stratified cumulative distributions of flare peak temperature for 57 flares from MIR disk stars with  $M < 2 M_{\odot}$  (thick solid), 38 from diskfree stars with  $M < 2 M_{\odot}$  (thick dotted), 15 from high-accretors with  $M < 2 M_{\odot}$  (thick dashed), 8 from MIR disk stars with  $M > 2 M_{\odot}$  (thin solid), and 12 from diskfree stars with  $M > 2 M_{\odot}$  (thin dotted). Legends indicate median values. KS test probabilities compare temperature distributions between non-disk and disk or high-accretor stars.

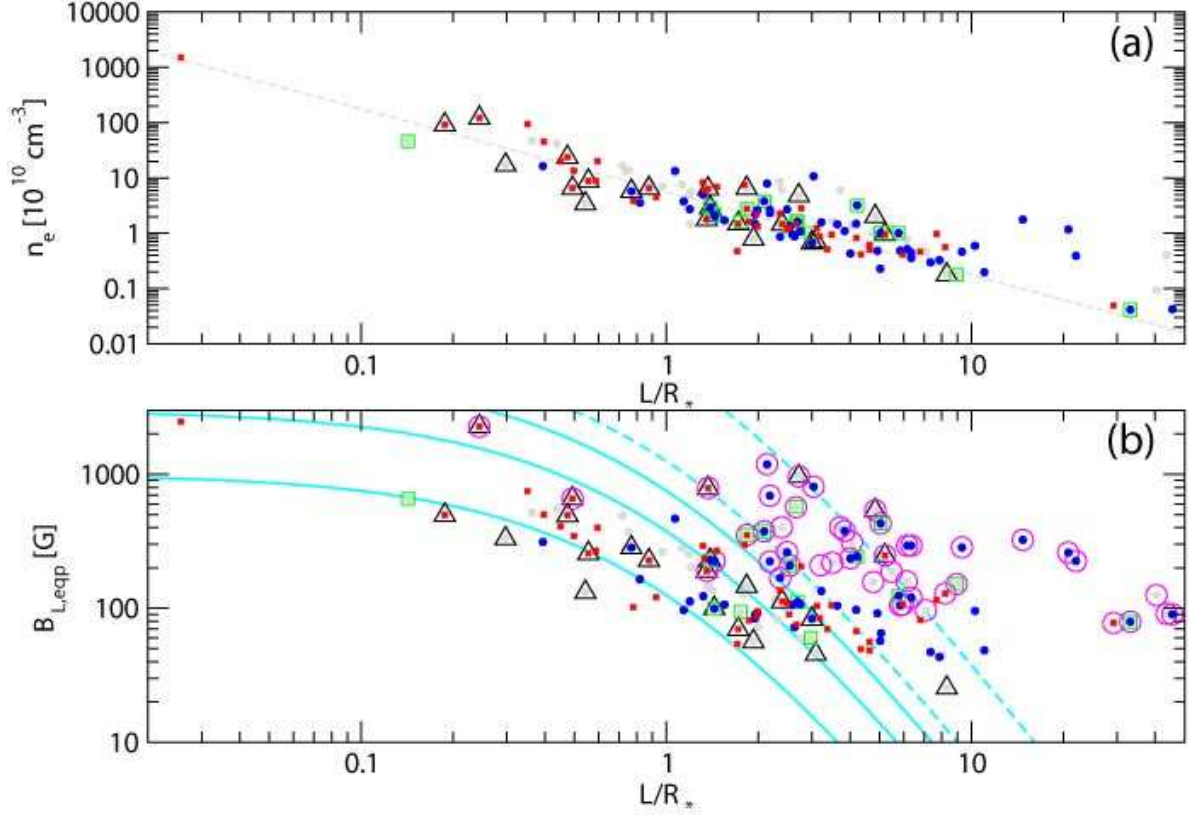


Fig. 11.— Estimated plasma density at flare peak (panel *a*) and magnetic field from pressure equipartition (panel *b*) are plotted against inferred loop sizes scaled to stellar radii. Symbols discriminate subsamples: MIR disk stars (blue circles); no MIR disk stars (red crosses); uncertain MIR disk stars (grey circles); highly accreting stars with  $EW(CaII) < -2 \text{ \AA}$  (green boxes); masses  $M > 2 M_{\odot}$  (black triangles); and super-hot flares with  $T_{obs,pk} > 100 \text{ MK}$  (magenta circles in panel *b*). In panel *a*, the dashed grey line indicates  $n_e \propto L^{-3/2}$ . In panel *b*, the cyan curves represent loci of photospheric dipolar magnetic fields  $B_{ph} = (1, 3, 6) \text{ kG}$  (solid) and  $(10, 50) \text{ kG}$  (dashed).

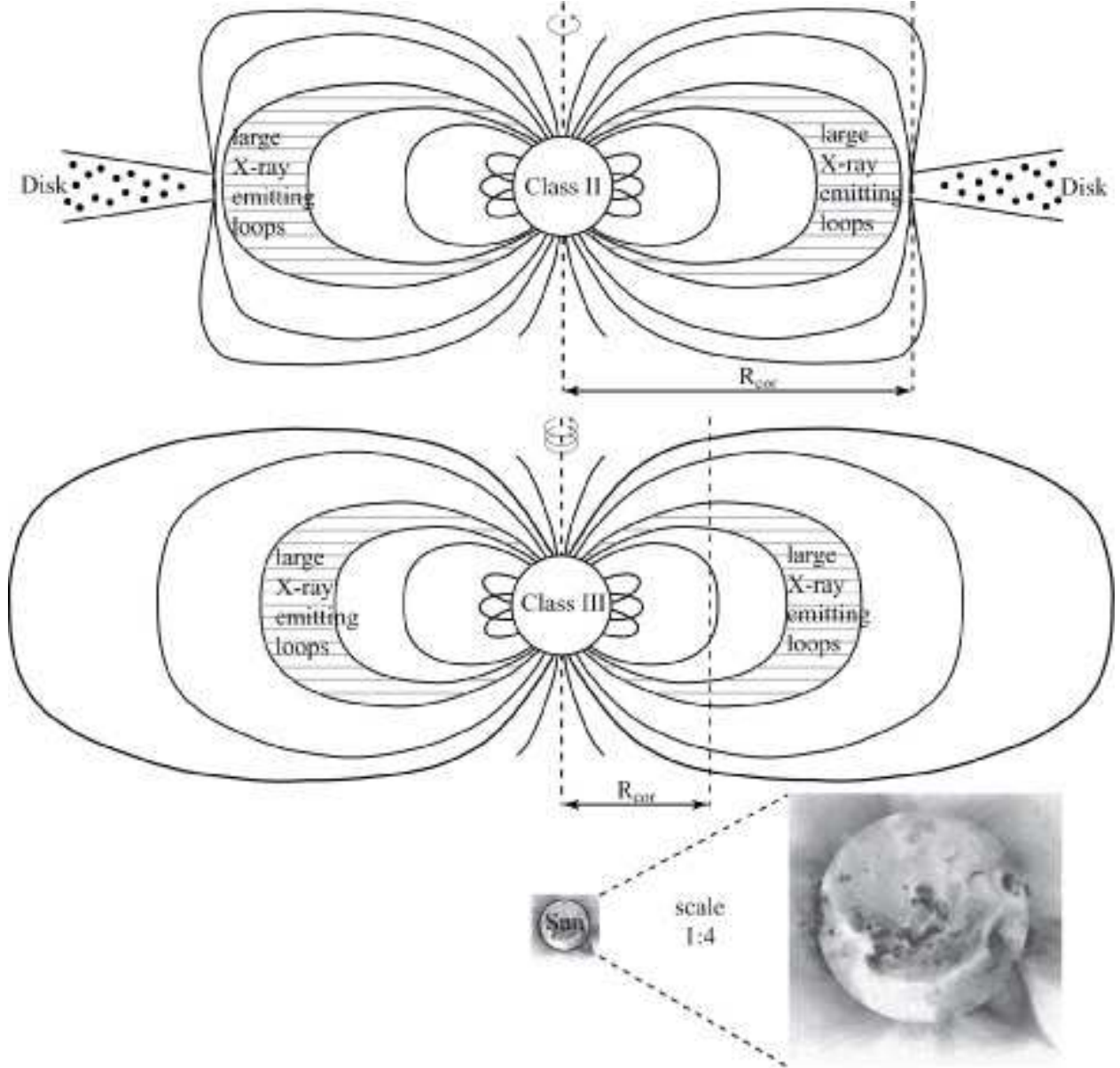


Fig. 12.— Sketch showing typical sizes of the largest X-ray emitting magnetic structures assuming a dipolar geometry (hatched) for Class II and Class III T-Tauri stars, respectively. Relative sizes are shown to scale for typical stars. The inset shows the X-ray image of the Sun, both to scale and expanded by a factor of 4 for clarity, showing a large helmet-like X-ray streamers (24 Jan 1992 flare, *Yohkoh* SXT).

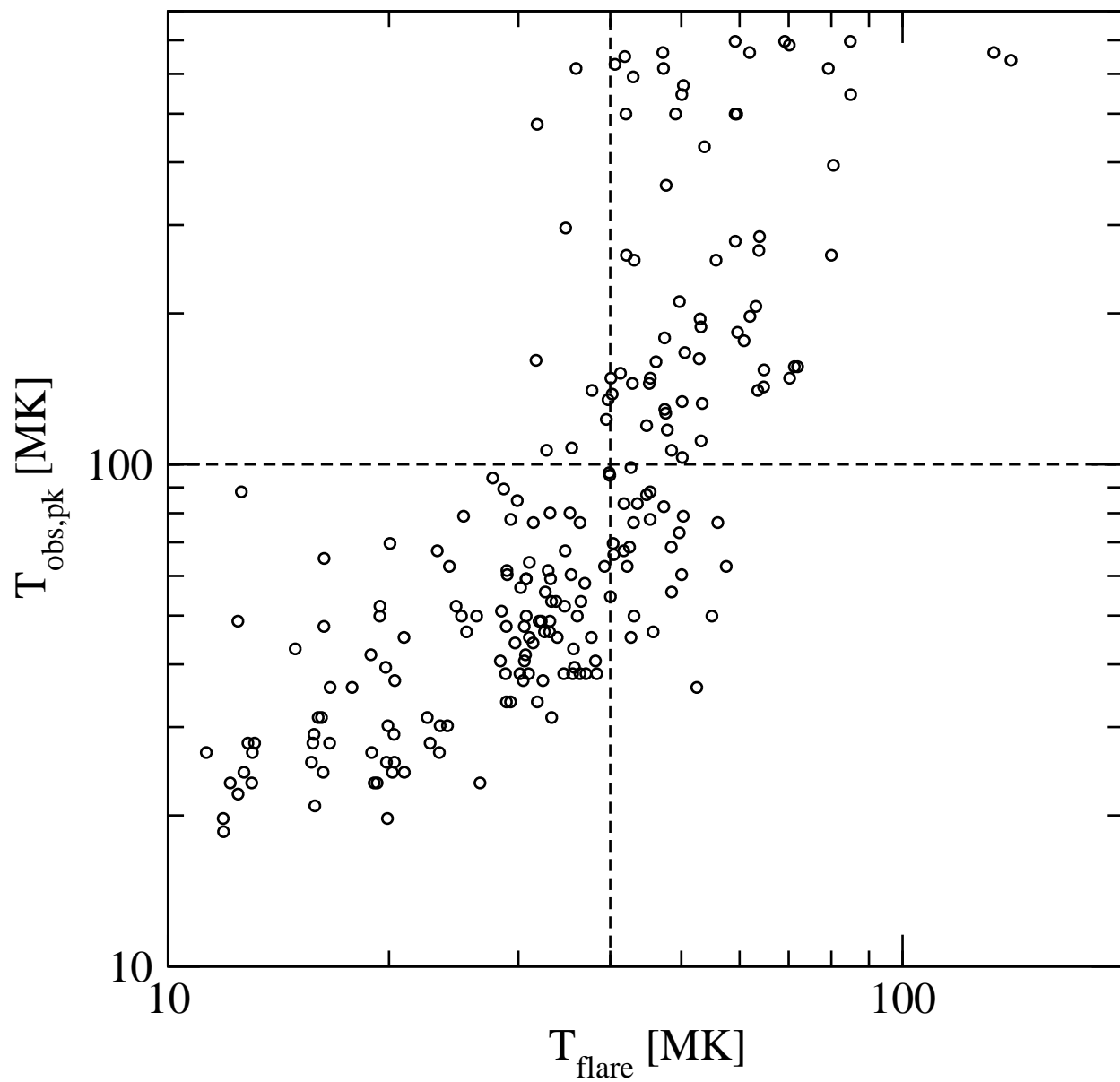


Fig. 13.— For all 216 COUP flares, comparison of the flare peak temperature from MASME analysis (Paper I) with the temperature derived from the spectral fit of the integrated flare spectrum. Dashed lines show 100 MK and 40 MK, respectively.

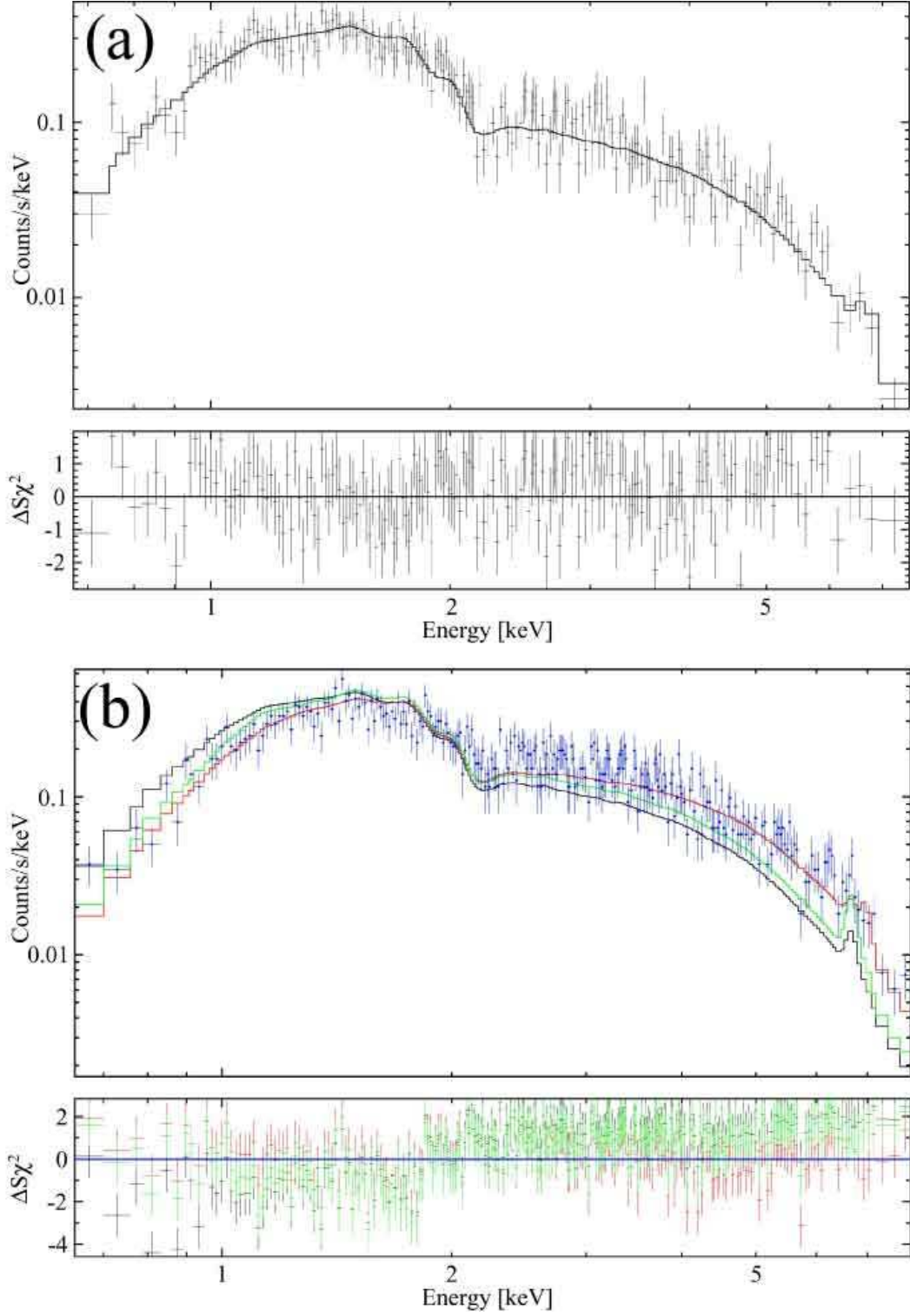


Fig. 14.— Composite flare peak spectra from MIR disk stars with source X-ray column densities in the narrow range of absorption. See Appendix for sample details. (a) Composite of 14 ordinary flares from 12 stars with  $T_{obs,pk} < 100$  MK. (b) Composite of 21 super-hot flares from 14 stars with  $T_{obs,pk} > 100$  MK. Three spectral models and residuals are: ordinary flare model (black), super-hot flare model (red), ordinary flare model with  $N_H$  fixed to that of super-hot model (green).